Revista Mexicana de Astronomía y Astrofísica, **54**, 1–20 (2018)

KIC 9451096: MAGNETIC ACTIVITY, FLARES AND DIFFERENTIAL ROTATION

O. Özdarcan, E. Yoldaş, and H. A. Dal

Ege University, Science Faculty, Department of Astronomy and Space Sciences, İzmir, Turkey

Received May 17 2017; accepted September 5 2017

ABSTRACT

We present a spectroscopic and photometric analysis of KIC 9451096. The combined spectroscopic and photometric modelling shows that the system is a detached eclipsing binary in a circular orbit and composed of F5V + K2V components. Subtracting the best–fitting light curve model from the whole long cadence data reveals additional low (mmag) amplitude light variations in time and occasional flares, suggesting a low, but still remarkable level of magnetic spot activity on the K2V component. Analyzing the rotational modulation of the light curve residuals enables us to estimate the differential rotation coefficient of the K2V component as $k = 0.069 \pm 0.008$, which is 3 times weaker compared with the solar value of $k = 0.19$, assuming a solar type differential rotation. We find the stellar flare activity frequency for the K2V component as 0.000368411 h^{-1} indicating a low magnetic activity level.

RESUMEN

Presentamos un análisis espectroscópico y fotométrico de KIC9451096. El modelo combinado muestra que el sistema es una binaria eclipsante separada, en órbita circular y compuesta de dos estrellas, F5V + K2V. Al sustraer la mejor curva de luz modelada de la cadencia completa de datos se revelan pequeñas variaciones en magnitud (mmag) así como ráfagas ocasionales, lo que sugiere una baja pero notable actividad de manchas magnéticas en la componente K2V. El análisis de la modulación rotacional de la curva de luz nos permite estimar que el coeficiente de la rotación diferencial de la componente K2V es $k = 0.069 \pm 0.008$, tres veces más débil que lel valor solar, $k = 0.19$. Encontramos que la frecuencia de la actividad de ráfagas en la K2V es 0.000368411 h^{-1}, lo que indica una baja actividad magnética.

Key Words: binaries: eclipsing — stars: activity — stars: flare — stars: fundamental parameters — stars: individual: KIC 9451096

1. INTRODUCTION

Although the primary aim of the *Kepler* mission is to detect transiting planets by obtaining very high precision photometric measurements, it provides further benefits, especially in terms of clear and reliable determination of very small amplitude light variations on eclipsing and intrinsic variable stars. About 150 000 targets have been observed in the mission, and apart from the exoplanets, numerous variable stars have been discovered. The unprecedented precision of the *Kepler* photometry clearly revealed low amplitude (mmag) light variations, which were used in the analysis of stellar flares, spot activity and differential rotation (Balona 2015; Balona et al. 2016; Reinhold & Reiners 2013; Reinhold et al. 2013a). Among these variable stars, 2876 eclipsing binary stars have been discovered (Prša et al. 2011; Slawson et al. 2011). Careful light curve modelling of the binaries with cool components ($T_{\rm eff} < 6500$ K) revealed rotational modulation of the light curves and flares in model residuals. KIC 09641031 (Yoldaş & Dal 2016), KIC 09761199 (Yoldaş & Dal 2017) and KIC 2557430 (Kamil & Dal 2017), GJ 1243, GJ 1245A and B (Hawley et al. 2014), KIC 2300039, KIC 4671547 (Balona 2015) are examples of such stars.

The analyses of the patterns of magnetic activity exhibited by these stars reveal some clues about

their evolutionary stages. Although there are several indicators found in these analyses, two of them are the energy spectra defined by Gershberg (1972) and the flare frequencies described by Ishida et al. (1991). Both of them have been computed, especially from the 1970's to the 1980's, in order to figure out the magnetic activity levels for the stars with detected flares. In 1990's, Leto et al. (1997) examined the flare frequency variation of EV Lac, a well-known UV Ceti type star. There are a few studies on the activity levels of three magnetic active stars discovered in the Kepler Mission depending on their flare frequencies. Yoldaş & Dal (2016) detected 240 flares from KIC 09641031, and Yoldaş & Dal (2017) detected 94 flares from KIC 09761199. In addition, Kamil & Dal (2017) detected 69 flares from KIC 2557430. Yoldaş & Dal (2016) derived the one phase exponential association (hereafter OPEA) model, and the flare frequency N_1 was found to be 0.41632 h^{-1} for KIC 09641031. Yoldaş & Dal (2017) computed N_1 as 0.01351 h^{-1} for 69 flares for KIC 09761199. However, an interesting situation occurs in the case of KIC 2557430. Kamil & Dal (2017) find that some of the flares detected from KIC 2557430 come from a third body; it is unclear whether it is a component in the system or an undetected background light source. Depending on the OPEA model derived from 69 flares, Kamil & Dal (2017) reveal that 40 (called Group 1) of them come from the secondary component, while 29 flares (called Group 2) come from a third body. They computed the flare frequency N_1 as 0.02726 h^{-1} for Group 1 and 0.01977 h^{-1} for Group 2. As discussed by Yoldaş & Dal (2016) and Gershberg (2005), the flare frequency is one of the parameters indicating the nature of the flare mechanism in the stellar atmosphere. Apart from the classical parameters described by Gershberg (2005), Dal & Evren (2010, 2011) have also described some new parameters derived from the OPEA models in order to determine the flare process occurring on the stellar surface.

Continuous photometry of variable single stars discovered by *Kepler* enabled to trace photometric period variations as a proxy of differential rotation via Fourier transform (see, e.g. Reinhold et al. 2013b; Reinhold & Reiners 2013). However, the Fourier transform may not perfectly work in case of eclipsing binaries, where the amplitude of the rotational modulation of star spots is usually embedded into the relatively large amplitude light variations caused by eclipses and the lack of spherical symmetry of the binary components. Furthermore, insufficient representation of light curve models, especially around mid-eclipse phases, may require discarding data around those phases and may cause regular gaps in the light curve, which would lead to unwanted alias periods and harmonics. In this case, alternative methods should be adopted to trace photometric period variation, such as an $O-C$ diagram based on minimum times of rotationally modulated light curves (see, e.g. Özdarcan et al. 2010).

In the case of eclipsing binary stars, additional intrinsic variations may not be determined at first, due to the reasons explained above. KIC 9451096 is such an eclipsing binary in the *Kepler* eclipsing binary catalog[1] (Prša et al. 2011; Slawson et al. 2011) with a short period, and with a confirmed third body (Borkovits et al. 2016). Beyond the properties provided by the catalog, such as morphology and eclipse depths, Armstrong et al. (2014) provided physical information, estimated from the spectral energy distribution based on photometric measurements. They estimated the effective temperature of the components of KIC 9451096 as 7166 K and 5729 K for the primary and the secondary component, respectively.

In this study, we carry out a photometric and spectroscopic analysis of KIC 9451096, based on *Kepler* photometry and optical spectroscopic observations with intermediate resolution described in § 2. § 3 describes the spectroscopic and photometric modelling of the system, and the analysis of the out–of–eclipse variations. In the final section, we summarize and discuss our findings.

2. OBSERVATIONS AND DATA REDUCTIONS

2.1. *Kepler Photometry*

Photometric data obtained by the *Kepler* spacecraft cover a broad wavelength range between 4100 Å and 9100 Å; this has the advantage of collecting many more photons in a single exposure and reaching sub-milli-mag precision, but also has the disadvantage of having no "true" photometric filter, hence no photometric color information. There are two types of photometric data having different exposure times. These are short cadence data (having an exposure time of 58.89 seconds) and long cadence data (having an exposure time of 29.4 minutes). In this study we use long cadence data of KIC 9451096 obtained from the *Kepler* eclipsing binary catalog. The catalog provides detrended and normalized intensities, which are obtained by application of procedures described by Slawson et al. (2011) and Prša et al. (2011). The whole data covers ≈4 years of time, with 65 307 data points in total. The MAST

[1] http://keplerebs.villanova.edu/

archive reports 0.9% contamination level in the measurements, practically indicating no additional light contribution to the measured fluxes of KIC 9451096.

2.2. *Spectroscopy*

We obtained optical spectra of KIC 9451096 with the 1.5 m Russian – Turkish telescope equipped with the Turkish Faint Object Spectrograph Camera[2] (TFOSC) at Tubitak National Observatory. TFOSC enables one to obtain intermediate resolution optical spectra in échelle mode. In our case, the instrumental setup provides actual resolution of $R = \lambda/\Delta\lambda \approx 2800$ around 6500 Å, and the observed spectra cover a usable wavelength range between 3900–9100 Å in 11 échelle orders. A back illuminated 2048 × 2048 pixels CCD camera, which has pixel size of 15 × 15 μm^2, was used to record spectra.

We obtained ten optical spectra of KIC 9451096 during the 2014 and 2016 observing seasons. In order to obtain enough signal, we used 3600 s of exposure time for each observation. The estimated signal–to–noise ratio (SNR) of observed spectra is mostly between 80–100, except for a few cases, where the SNR is around 50. SNR estimation is based on photon statistic. Together with the target star, we also obtained high SNR optical spectra of HD 225239 (G2V, $v_r = 4.80\,\mathrm{km\,s^{-1}}$) and ι Psc (HD 222368, F7V, $v_r = 5.656\,\mathrm{km\,s^{-1}}$), and adopted them as radial velocity and spectroscopic comparison templates.

We reduced all observations using standard IRAF[3] packages and tasks. A typical reduction procedure starts with obtaining a master bias frame from several bias frames taken nightly, and subtracting the master bias frame from all object, calibration lamp (Fe-Ar spectra in our case) and halogen lamp frames. Then the bias corrected halogen frames are combined to form an average halogen frame and this average frame is normalized to unity to produce the normalized master flat frame. After that, all target and calibration lamp spectra are divided by the normalized flat field frame. Next, cosmic rays removal and scattered light corrections are applied to the bias and flat corrected frames. At the end of these steps, reduced frames are obtained and these frames are used for the extraction of spectra. In the final steps, Fe-Ar frames are used for wavelength calibration of the extracted spectra and the wavelength calibrated spectra are normalized to unity by using cubic spline functions.

[2] `http://www.tug.tubitak.gov.tr/rtt150_tfosc.php`

[3] The Image Reduction and Analysis Facility is hosted by the National Optical Astronomy Observatories in Tucson, Arizona at URL iraf.noao.edu.

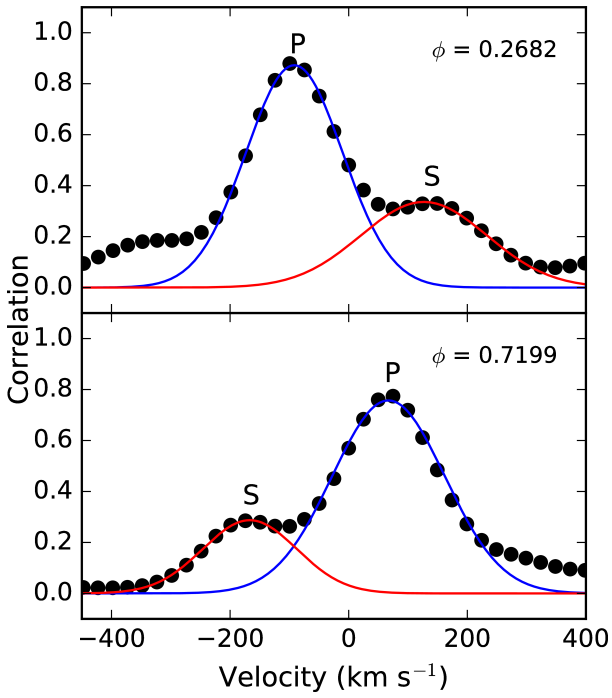

Fig. 1. Cross-correlation functions of two spectra obtained around orbital quadratures. The letter ϕ denotes corresponding orbital phase. P and S indicate the primary component and the secondary component, respectively.

3. ANALYSIS

3.1. *Radial Velocities and Spectroscopic Orbit*

The first step of our analysis is to determine the radial velocities of the components and the spectroscopic orbit of the system. We cross-correlated each observed spectrum of KIC 9451096 with spectra of template stars HD 225239 and ι Psc, as described in Tonry & Davis (1979). In practice we used the *fxcor* task in IRAF environment. We achieved better cross-correlation signals (especially for the weak secondary component) when we used HD 225239 as template; thus, we determined all radial velocities with respect to the HD 225239 spectrum. We obtained acceptable cross-correlation signals of both components in échelle orders 5 and 6, which cover a wavelength range between 4900–5700 Å. Figure 1 shows the cross-correlation functions of two spectra obtained around orbital quadratures.

We list the observation log and the measured radial velocities of the components in Table 1. Note that we use the ephemeris and period given by

TABLE 1

LOG OF SPECTROSCOPIC OBSERVATIONS*

HJD (24 00000+)	Orbital Phase	Exposure time (s)	Primary V_r	Primary σ	Secondary V_r	Secondary σ
56842.5435	0.7794	3600	91.4	8.2	-152.5	36.9
56844.4052	0.2682	3600	-79.9	6.3	151.9	39.1
56844.4479	0.3024	3600	-74.4	6.6	155.0	37.2
56889.4315	0.2781	3600	-77.1	5.7	148.1	40.0
56890.2958	0.9693	3600	14.5	5.0	—	—
57591.4532	0.7199	3600	88.5	7.2	-153.3	32.0
57601.4386	0.7058	3600	88.7	5.4	-149.8	32.1
57616.4778	0.7333	3600	86.0	4.3	-145.2	38.7
57617.5188	0.5659	3600	31.0	5.8	—	—
57672.3009	0.3779	3600	-54.8	5.1	111.1	47.9

*together with measured radial velocities and their corresponding standard errors (σ) in km s^{-1}.

Borkovits et al. (2016) and listed in their Table 2 to calculate orbital phases and for further analysis.

We achieved a reasonable solution for the spectroscopic orbit assuming zero eccentricity, where an undefined longitude of periastron is taken. We checked this assumption by inspecting the *Kepler* light curve of the system, where we observe deeper and shallower eclipses at 0.0 and 0.5 orbital phases, respectively, indicating a circular orbit (see § 3.3, Figure 4). In order to reach the final spectroscopic orbital solution, we prepared a simple script written in Python language, which applies Markov chain Monte Carlo simulations to the measured radial velocities, considering their measured errors. We list the final spectroscopic orbital elements in Table 2 and plot the measured radial velocities, their observational errors, the theoretical spectroscopic orbit and residuals from the solution in Figure 2.

3.2. *Spectral Type*

We rely on our intermediate resolution TFOSC optical spectra to determine the spectral type of the components. Most of our spectra correspond to the phases around orbital quadratures, where we observe the signal of the two components separated. However, there are two spectra obtained at phases close to the eclipses, where the two components can not be resolved separately. One of these spectra corresponds to ≈ 0.56 orbital phase (see Table 1), where we cannot observe the radial velocity signal of the secondary component in cross-correlation. Even at the orbital quadratures, the cross-correlation signal of the secondary component is considerably weak

TABLE 2

SPECTROSCOPIC ORBITAL ELEMENTS OF KIC 9451096.*

Parameter	Value
$P_{\rm orb}$ (day)	1.25039069 (fixed)
T_0 (HJD24 00000+)	54954.72942 (fixed)
γ (km s^{-1})	2.8±0.5
K_1 (km s^{-1})	84.1±2.3
K_2 (km s^{-1})	153.2±14.6
e	0 (fixed)
$a \sin i$ ($R_\odot$)	5.92±0.35
$M \sin^3 i$ ($M_\odot$)	1.79±0.25
Mass ratio ($q = M_2/M_1$)	0.55±0.05
rms1 (km s^{-1})	3.7
rms2 (km s^{-1})	4.9

*M_1 and M_2 denote the masses of the primary and the secondary component, respectively, while M shows the total mass of the system.

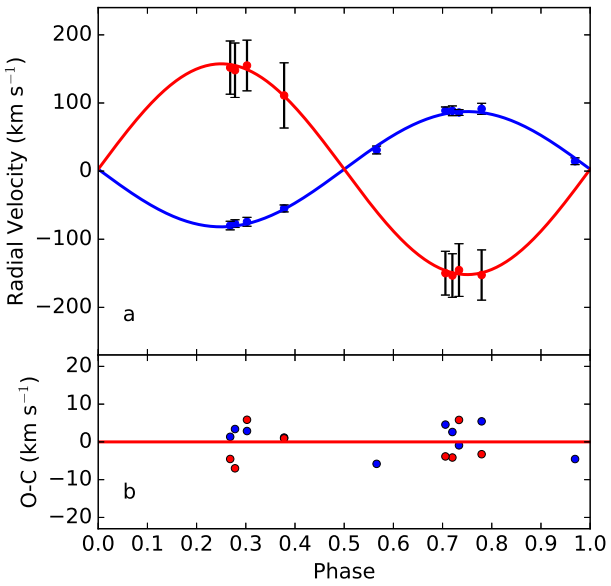

Fig. 2. (a) Observed radial velocities of the primary and the secondary (blue and red filled circles, respectively), and their corresponding theoretical representations (blue and red curve). (b) Residuals from theoretical solution. The color figure can be viewed online.

compared to the primary component, indicating a very small light contribution from the secondary component to the total light of the system. Our preliminary light curve analysis shows that the contribution of the secondary component to the total

light does not exceed ≈ 10%. In this case, the signal from the secondary component becomes almost negligible at the resolution of our observed spectrum at ≈ 0.56 orbital phase. Therefore, we assume that we only observe the spectrum of the primary component and adopt this spectrum as reference spectrum for the primary component. We confirm this assumption by calculating the composite spectrum of the binary via final parameters of the components (see § 3.3), where we observe that the contribution of the secondary component affects the theoretical composite spectrum less than 2% for the wavelength range of 4900-5700 Å. We refrain from performing a detailed analysis with spectral disentangling. Future studies could take advantage of this technique and derive atmospheric parameters of the secondary.

We first compare the reference spectrum with the template spectra of HD 225239 and ι Psc. We observe that ι Psc spectrum provides a closer match to the reference spectrum but also indicates earlier spectral type and slightly lower metal abundances for the primary component. At that point, we switch to the spectrum synthesizing method. We use the latest version of python framework *iSpec* (Blanco-Cuaresma et al. 2014) which enables practical and quick calculation of a synthetic spectrum with a given set of atmospheric parameters via different radiative transfer codes. Among these codes we adopt the SPECTRUM[4] code (Gray & Corbally 1994), together with ATLAS-9 (Castelli & Kurucz 2004) model atmospheres and the actual line list from the third version of the Vienna atomic line database (*VALD*3, Ryabchikova et al. 2015).

Considering the spectral type of ι Psc, we synthesize spectra for effective temperatures between 6000 K and 7000 K in steps of 250 K, and metallicity values ([Fe/H]) between −1.0 and 0.0 in steps of 0.5. For all synthetic spectra we fix the gravity ($\log g$) to 4.15, which we precisely calculate by light curve modelling (see § 3.3). Since we do not have a high resolution spectrum, we fix the microturbulence velocity to 2 km s^{-1}. We convolve all calculated spectra with a proper Gaussian line spread function in order to degrade their resolution to the resolution of the TFOSC spectra. Instrumental broadening in TFOSC spectra is 2.2 Å, corresponding 119 km s^{-1} for wavelengths around 5500 Å. The estimated projected rotational velocities of the components are 62 km s^{-1} and 36 km s^{-1} for the primary and the secondary component respectively (see § 3.3). Since instrumental broadening is the most dominant broadening source in the observed spectra, we do not consider rotational broadening and other line broadening mechanisms.

Among the calculated spectra we find that the model with 6500 K effective temperature and an [Fe/H] value of −0.5 provides the closest match to the reference spectrum. The final effective temperature indicates F5 spectral type (Gray 2005). Considering the effective temperature and metallicity steps in model atmospheres, and the resolution of TFOSC spectra, the final values and their estimated uncertainties are $T_{\rm eff}$ = 6500±200 K and [Fe/H] = −0.5±0.5 dex, respectively. Note that even if we considered the neglected contribution of the secondary component in the reference spectrum, its effect would be within the estimated uncertainties above. The final $T_{\rm eff}$ value is ≈ 670 K lower than the 7166 K value estimated in Armstrong et al. (2014). In Figure 3 we show portions of the reference spectrum and the model spectrum, calculated with the final parameters above.

3.3. *Light Curve Modelling and Physical Properties*

Global visual inspection of KIC 9451096 *Kepler* photometry reflects properties of a typical close eclipsing binary. We start the light curve modelling by phasing the whole long cadence data with respect to the ephemeris and period given by Borkovits et al. (2016), and re–binning the phased data with a phase step of 0.002 via the freely the available fortran code *lcbin*[5] written by John Southworth. We plot the binned and phased light curves of the system in Figure 4, panels *a* and *aa*. The light curve indicates a detached configuration for the system. Mid-eclipse phases are 0.0 and 0.5 phases, indicating a circular orbit. There is no conspicuous asymmetry in the light curve.

We model the light curve with the 2015 version of the Wilson-Devinney code (Wilson & Devinney 1971; Wilson & Van Hamme 2014). In the modelling, we first fix the most critical two parameters of the light curve modelling, i.e., the mass ratio (q) of the system and the effective temperature of the primary component (T_1). Since we have reliably derived these parameters in previous sections as q = 0.55 and T_1 = 6500 K, we adopt them as fixed parameters. The calculated atmospheric properties of the primary component reveal that both stars have convective envelopes. Therefore, we set albedo (A_1, A_2) and gravity darkening (g_1, g_2) coefficients of the com-

[4] http://www.appstate.edu/~grayro/spectrum/spectrum.html

[5] http://www.astro.keele.ac.uk/~jkt/codes.html#lcbin

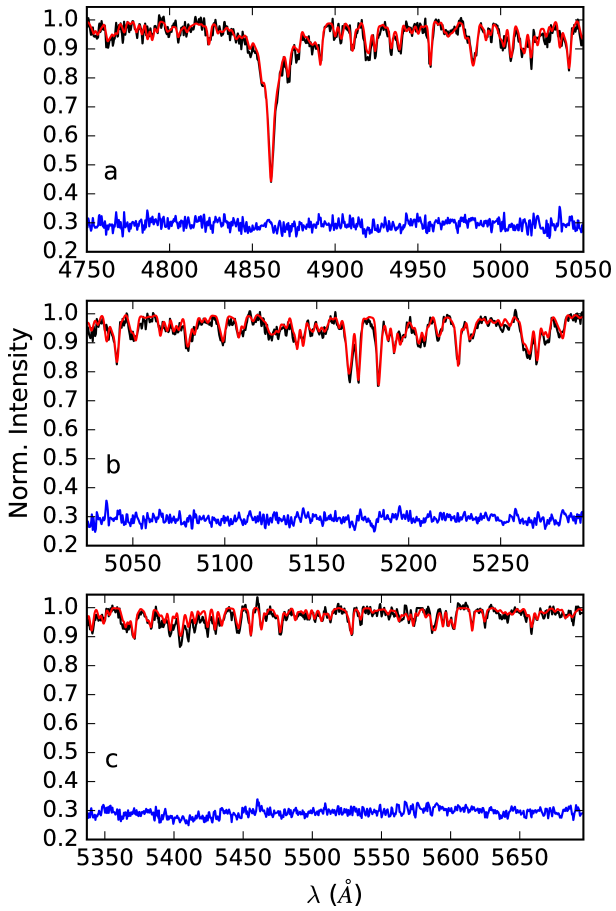

Fig. 3. Representation of the observed (black), best matched (red) synthetic spectrum and residuals (blue) for three regions. Note that we shift the residuals upwards by 0.3 for the sake of simplicity. Panels *a*, *b* and *c* show the regions around H_β, Mg I triplet and metallic absorption lines around 5500 Å, respectively. The color figure can be viewed online.

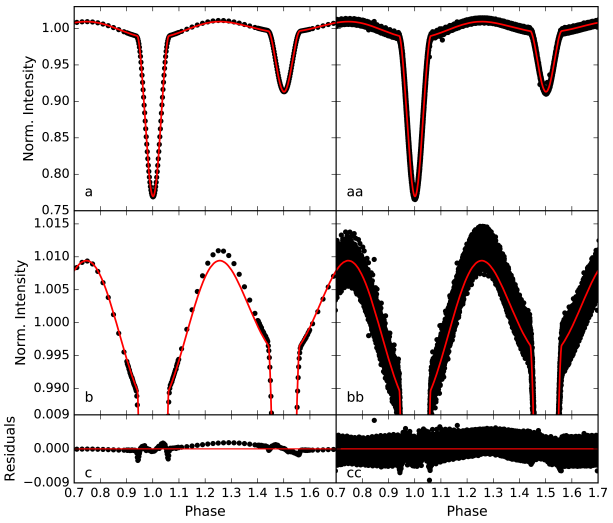

Fig. 4. (a) Phase binned light curve of KIC 9451096 (black filled circles) together with best-fitting model (red curves). (b) Close up view of the light curve at light maxima. **c)** Residuals from the best–fitting model. Panels at right (*aa*, *bb* and *cc*) are the same as left panels but for phased long cadence data. The color figure can be viewed online.

ponents to 0.5 and 0.32, respectively, which are typical values for stars with convective outer envelopes. We also consider a slight metal deficiency of the system, and thus adopt the internal stellar atmosphere formulation of the Wilson-Devinney code according to the determined [Fe/H] value of −0.5. We assume that the rotation of the components is synchronous with the orbital motion, and thus fix the rotation parameter of each component (F_1, F_2) to 1.0. We adopt a square root law (Klinglesmith & Sobieski 1970) for limb darkening of each component; this is more appropriate for stars cooler than 9000 K. We take the limb darkening coefficients for the *Kepler* passband (x_1, x_2, y_1, y_2) and the bolometric coefficients (x_{1bol}, x_{2bol}, y_{1bol}, y_{2bol}) from van Hamme (1993). In the modelling, we adjust inclination of the orbit (i), temperature of the secondary component (T_2), dimensionless omega potentials of the components (Ω_1, Ω_2) and luminosity of the primary component (L_1). We also include a phase shift parameter as adjustable in the modelling, since we expect a shift in the ephemeris due to the light–time effect of the third body (Borkovits et al. 2016). The model quickly converged to a steady solution in a few iterations. We list the model output in Table 3 and we plot the best–fitting model in Figure 4, panels *a*, *b*, and the residuals from the model in panel *c*.

In Figure 4, panel *b*, one can easily see the model inconsistency around 0.25 orbital phase. The inconsistency indicates an additional light variation, which is known as $O'Connell\ effect$, i.e. difference between light levels of subsequent maxima in an orbital cycle. Possible sources of the difference may be Doppler beaming, a hot spot or a cool spot on one of the component of the system. KIC 9451096 is a detached eclipsing binary, thus we can safely exclude possibility of mass transfer between components, i.e., a hot spot possibility. Doppler beaming was detected observationally among some *Kepler* binaries (see, e.g. van Kerkwijk et al. 2010), which becomes important for systems with very low mass ratios, especially for systems with a compact component, such as a white dwarf or a hot sub-dwarf. In addition,

TABLE 3

LIGHT CURVE MODELLING RESULTS OF KIC 9451096.[a]

Parameter	Value
q	0.55*
$T_1(K)$	6500*
g_1, g_2	0.32*, 0.32*
A_1, A_2	0.5*, 0.5*
$F_1 = F_2$	1.0*
phase shift	0.00108(2)
i (°)	79.07(4)
$T_2(K)$	5044(200)
Ω_1	4.4942(49)
Ω_2	4.8885(125)
$L_1/(L_1+L_2)$	0.897(1)
x_1bol, x_2bol	0.136*, 0.293*
y_1bol, y_2bol	0.583*, 0.401*
x_1, x_2	0.106*, 0.482*
y_1, y_2	0.670*, 0.313*
$\langle r_1\rangle, \langle r_2\rangle$	0.2557(3), 0.1506(5)
Model rms	3.0×10^{-4}

[a] $\langle r_1\rangle$ and $\langle r_2\rangle$ denote the mean fractional radii of the primary and the secondary components, respectively. Internal errors of the adjusted parameters are given in parentheses for the last digits. Asterisk symbols in the table denote fixed values for the corresponding parameter. Note that we adopt the uncertainty of T_1 for T_2 as well, since the internal error of T_2 is unrealistically small ($\sim$1 K).

if the effect is in progress, then it would change the light levels of each maxima. However, we observe inconsistency only for phase 0.25, while the model fairly represents the light level at phase 0.75. Thus, Doppler beaming should have a negligible effect in the case of KIC 9451096, if any. A remaining possibility is cool spots located preferably on the cooler component.

Here we do not chose to model this inconsistency alone, which would only show the cumulative effect of hundreds of light curves, but instead we subtract the best–fitting model from the whole long cadence data and inspect the residuals in order to investigate further light variations. We will focus on this in § 3.4.

We complete the light curve modelling section with a calculation of the absolute parameters of the system by combining the spectroscopic orbital solution and light curve model results. In Table 4, we give the physical properties of each component. Our analysis reveals that the system is formed by an F5V primary and a K2V secondary component.

TABLE 4

ABSOLUTE PHYSICAL PROPERTIES OF KIC 9451096.*

Parameter	Primary	Secondary
Spectral Type	F5V	K2V
[Fe/H]	-0.5 ± 0.5	
Mass ($M_\odot$)	1.18(26)	0.65(9)
Radius ($R_\odot$)	1.53(10)	0.90(6)
Log $L/L_\odot$	0.574(76)	−0.327(88)
log g (cgs)	4.14(4)	4.34(1)
M_{bol} (mag)	3.31(19)	5.57(22)

*The error of each parameter is given in parantheses for the last digits.

3.4. *The Out-of-Eclipse Variations*

In this section, we subtract the best–fitting light curve model from the whole long cadence data and obtain residuals. Here, we first divide the whole long cadence data into subsets, where each subset covers only a single orbital cycle, resulting in 1026 individual light curves. Then we apply the differential corrections routine of the Wilson-Devinney code and fix all parameters, except the ephemeris reference time. In this way, we find a precise ephemeris reference time for each individual subset, therefore eliminating any shift in the ephemeris time due to the third body reported by Borkovits et al. (2016), and obtain precise residuals. In Figure 5, we plot three different parts of the residuals. Note that we remove data points that correspond to the eclipse phases due to the insufficient representation of the model at those phases. This mainly arises from the inadequacy of radiative physics used in light curve modelling for a very high photometric precision and can clearly be seen in Figure 4 panel *c*.

Inspecting residual brightness, we immediately see a variation pattern which changes its shape from time to time. Furthermore, we observe a sudden increase and gradual decrease in the residual brightness which occasionally occurs over four years of time span and has short time scale of a few hours. These patterns are traces of magnetic spot activity, which is very possible for the K2V secondary component. Observational confirmation of this possibility can be done by inspecting magnetic activity sensitive spectral lines, such as the H_α and Ca II H & K

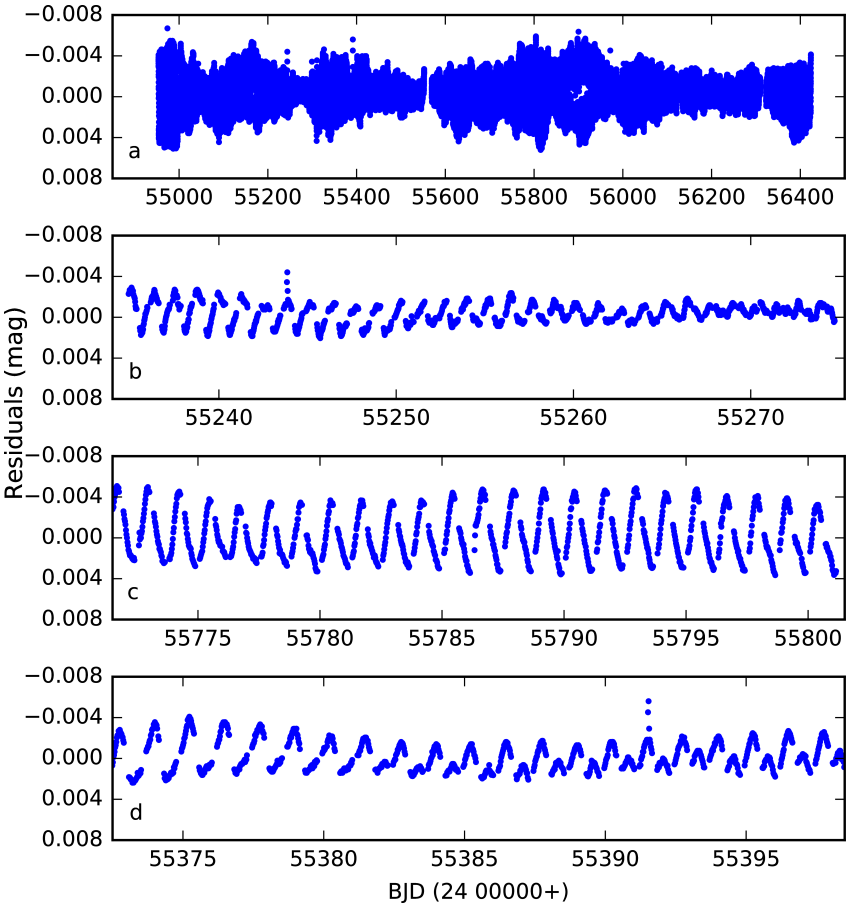

Fig. 5. (a) Residuals from whole long cadence data. Remaining panels show different time ranges of residuals, where we observe different light curve shapes, and flares.

lines. We inspected these lines in our TFOSC spectra and did not notice any emission features, which could be considered as the sign of the activity. However, one should consider that the contribution of the secondary component to the total light does not exceed 10% at optical wavelengths and will steeply decrease towards the ultraviolet region of the spectrum. Furthermore, the variation patterns observed in Figure 5 exhibit very small amplitudes. Therefore, the existence of magnetic spot activity cannot be confirmed or excluded via spectral line inspection in the case of KIC 9451096. Nevertheless, variation patterns and flares observed in the residuals indicate weak magnetic spot activity in the secondary component, which can still be detected with the very high precision of the *Kepler* photometry.

We analyze rotational modulation and flares of the secondary component via residuals by assuming that the source of all variation patterns is only the secondary component.

3.4.1. *Photometric Period and Differential Rotation*

Conventional periodogram methods for determining rotational period do not perfectly work in our case because the observed variation patterns exhibit quick changes in amplitude and mean brightness level over short time scales of a few days, which is comparable to the orbital period. Moreover, since we remove data points at eclipse phases, this causes regular gaps in the data which repeat each ≈ 0.625 day (i.e. half of the orbital period); thus, it causes an alias period and its harmonics, and disturbs the real periods. Furthermore, one can clearly see that the rotational modulation of residuals has an asymmetric shape. Considering an individual light curve with an asymmetric shape, it is not possible to find a single period to represent the whole light curve perfectly, and additional periods (i.e. harmonics) are required. Therefore we apply an alternative method based on tracing the time of a minimum light observed in an orbital cycle, which was previously ap-

plied to RS CVn system HD 208472 (Özdarcan et al. 2010). For each orbital cycle, we find the time of the deepest minimum in the cycle by fitting a second or third order polynomial to the data points around the expected minimum time. The order of the polynomial depends on the light curve shape. After obtaining all minimum times, we construct an $O-C$ diagram by adopting the first minimum time observed in the residuals as initial ephemeris reference time, and the orbital period as the initial period, and obtain $O-CI$ values. Then we apply a linear fit to the $O-CI$ values and calculate an average ephemeris reference time and period given in Equation 1, together with statistical uncertainties given in parentheses for the last digits.

$$T_0(\mathrm{BJD}) = 2,454,954.02(24) + 1\overset{\mathrm{d}}{.}24544(36) \times E. \quad (1)$$

In the equation, T_0(BJD) and E denote ephemeris reference time and integer cycle number, respectively. We plot $O-CI$ values and linear fit in Figure 6, panel *a*. After obtaining an average ephemeris and period, we subtract the linear fit from $O-CI$ data and obtain $O-CII$ data, which in principle shows the real period variation for a given time range. Figure 6, panel *b* shows $O-CII$ data. We divide $O-CII$ data into 30 subsets by grouping data points that appear with a linear slope. The linear trend of a subset gives the difference between the best–fitting photometric period of the subset and the grand average photometric period given in Equation 1. Therefore we can calculate a mean photometric period for each subset. We plot the calculated mean photometric periods versus time in Figure 6, panel *c*, together with the statistical uncertainties. We list photometric periods for 30 subsets in Table 5, and tabulate our $O-C$ analysis results in Table 8.

The average period given in Equation 1 represents the average rotation period for magnetic activity features on the surface of the secondary component, which are typically cool and dark regions, i.e., star spots, and indicates a slightly (∼0.5% day) shorter period compared to the orbital period. This is clearly observed in Figure 6 panel *c*, where the mean photometric periods of subsets are mostly shorter than the orbital period. Assuming a solar type differential rotation, this means that the orbital period is slightly longer than the equatorial rotation period of the secondary component. Under the same assumption, the differential rotation coefficient can be estimated from $(P_{max}-P_{min})/P_{equ} = kf$, where P_{max}, P_{min}, k and f denote observed maximum and minimum period, differential rotation coefficient and a constant that depends on the range of spot forming latitudes, respectively (Hall & Busby 1990). Considering the small amplitude of rotational modulation of residuals, we assume that the secondary component is not largely spotted and that the total latitudinal range of the spot distribution is 45 degrees, which causes the f constant to take values between 0.5 and 0.7 (Hall & Busby 1990). Using maximum and minimum photometric periods from the $O-C$ analysis, and assuming that the shortest period corresponds

TABLE 5

PHOTOMETRIC PERIODS FOUND FROM $O-C$ ANALYSIS

Subset	BJD (24 00000+)	P (day)	σ(P) (day)
1	54994.8107	1.2456	0.0004
2	55048.8731	1.2326	0.0008
3	55094.1598	1.2441	0.0004
4	55139.0644	1.2260	0.0019
5	55169.9192	1.2459	0.0008
6	55208.0721	1.2489	0.0006
7	55250.0831	1.2584	0.0011
8	55314.8252	1.2484	0.0004
9	55366.4562	1.2355	0.0006
10	55425.0957	1.2470	0.0006
11	55478.0779	1.2517	0.0010
12	55507.4240	1.2437	0.0006
13	55539.3828	1.2216	0.0025
14	55629.1787	1.2430	0.0004
15	55702.5236	1.2447	0.0004
16	55740.2684	1.2522	0.0007
17	55793.0150	1.2485	0.0004
18	55840.9410	1.2223	0.0022
19	55868.2947	1.2534	0.0005
20	55894.6874	1.2712	0.0022
21	55924.7567	1.2494	0.0006
22	55960.4676	1.2391	0.0011
23	55996.8636	1.2507	0.0005
24	56026.2172	1.2474	0.0009
25	56073.0738	1.2528	0.0005
26	56136.3924	1.2449	0.0005
27	56258.6328	1.2509	0.0004
28	56333.3104	1.2323	0.0019
29	56359.5423	1.2565	0.0008
30	56400.8932	1.2504	0.0004

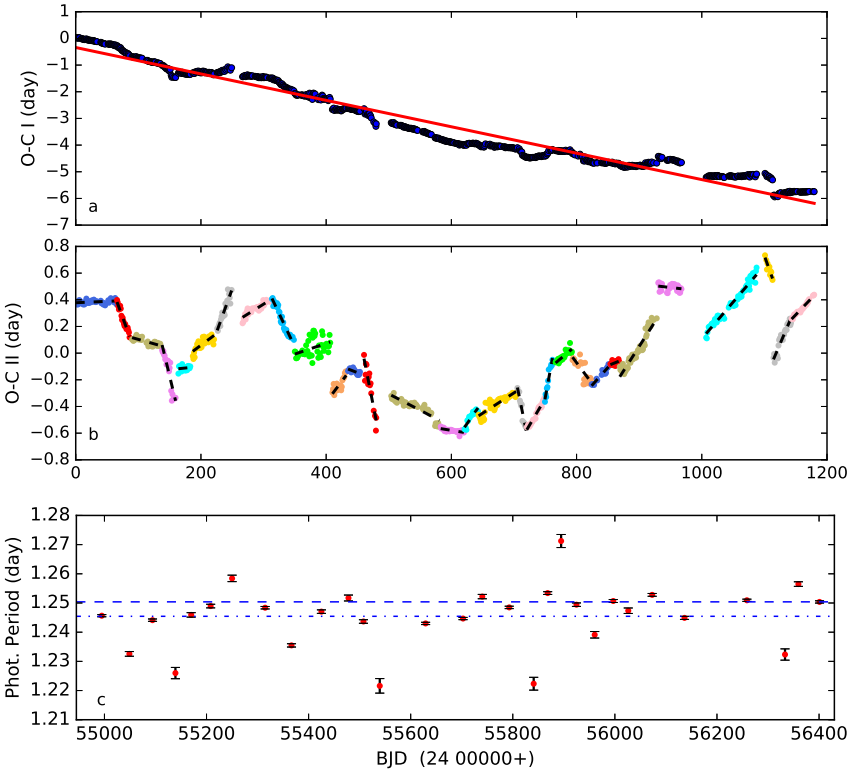

Fig. 6. (a) $O-CI$ diagram of observed minimum times (blue filled circles) and linear fit (red line). (b) $O-CII$ diagram obtained via residuals from the linear fit in panel a. Each color denotes a subset where data points appear on a linear trend. The linear fit to each subset is shown by a black dashed line. (c) Calculated mean photometric period for each subset (red filled circles) and the statistical uncertainties. Note that the horizontal axis values are converted from E numbers to barycentric Julian date. Orbital period and grand average photometric period obtained from linear fit to the $O-CI$ data are shown with blue color as a dashed line and a dot–dashed line, respectively. The color figure can be viewed online.

to the equatorial rotation period of the star, we find $k = 0.081 \pm 0.011$ and $k = 0.058 \pm 0.006$ for $f = 0.5$ and $f = 0.7$, respectively. Since these k values are calculated via boundary values of f, the real differential rotation coefficient must lie in the range of k values calculated above. An average k is found as 0.069±0.008.

3.4.2. *Flares*

We detect 13 flares in the residuals from long cadence data. In the flare analysis, it is critical to determine the quiescent level, which denotes the brightness level in the absence of a flare. In our case, we determine the quiescent level by applying Fourier analysis to the single orbital cycle where the flare occurs. The Fourier analysis represents the rotational modulation of residuals in the cycle, and then we remove the Fourier representation from the data. The remaining residuals show only the quiescent level and the flare itself. We show such a flare light curve in Figure 7.

The energy (E) is a very important parameter for a flare. However, the energy parameter has the luminosity L of the star as a factor in equation $E = P \times L$ described by Gershberg (1972). Due to the disadvantages described in Dal & Evren (2010), we use the flare equivalent duration instead of the flare energy, which is more proper. We compute the equivalent durations of flares via the equation $P = \int[(I_{flare} - I_0)/I_0]dt$ (Gershberg 1972), where P is the flare equivalent duration in seconds, I_0 is the quiescent level intensity, and I_{flare} is the intensity observed at the moment of the flare. Considering the quiescent level, the times of flare beginning, flare maximum and flare end are determined, together with flare rise duration, flare decay duration and flare amplitude. We list all computed values in Table 6 for each of the 13 flares.

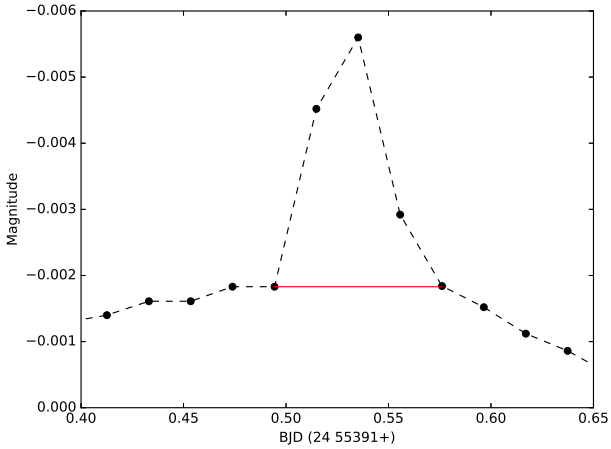

Fig. 7. An example of a flare light curve. The filled black circles represent the observations, while the red line represents the quiescent level derived from the data out-of-flare. The color figure can be viewed online.

TABLE 6

THE PARAMETERS CALCULATED FOR EACH FLARE.*

BJD (24 00000+)	P (s)	T_r (s)	T_d (s)	Amp (mag)
55021.2171	11.4	1763	15889	-0.001516
55043.1016	5.6	1763	5296	-0.002483
55310.6569	7.6	1763	8830	-0.002047
55326.5140	2.7	1771	1763	-0.001618
55412.0302	5.9	1763	7068	-0.001648
55416.9343	12.1	1771	14118	-0.002853
55824.2162	4.3	1763	5296	-0.001578
55931.1213	4.5	3534	3534	-0.001453
55971.7021	4.9	1763	5296	-0.002152
56142.9809	6.0	3534	7059	-0.001983
56284.8887	3.4	1771	3525	-0.001806
56286.5642	4.4	1771	3525	-0.001568
56375.4705	2.2	1763	1763	-0.001429

*Note that BJD column denotes the mid–flare time. T_r, T_d and Amp denote flare rise duration, flare decay duration and flare amplitude, respectively.

Dal & Evren (2010, 2011) suggest that the best function to represent the relation between flare equivalent duration and flare total duration is the OPEA, where the flare equivalent duration is considered on a logarithmic scale. The OPEA function is defined as $y = y_0 + (Plateau - y_0) \times (1 - e^{-kx})$,

TABLE 7

PARAMETERS DERIVED FROM THE OPEA MODEL*

Parameter	Value
Y_0	-0.015961 ± 0.13891
Plateau	1.2394 ± 0.14441
K	$0.00011438 \pm 0.000036715$
Half-time	6060
R^2	0.94535
P value	~ 0.10

*Using the least squares method.

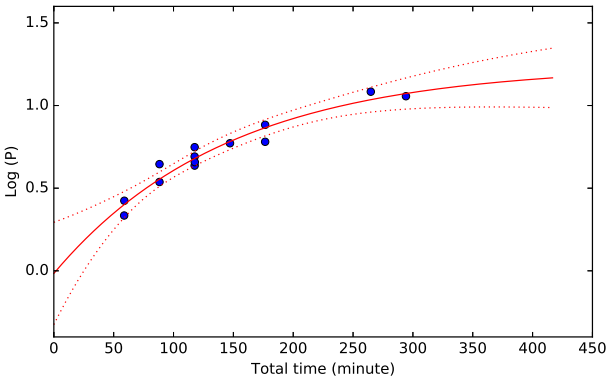

Fig. 8. The OPEA model obtained over 13 flares. The blue filled circles show each flare while the continuous red line shows the OPEA model and the dotted red lines show the sensitivity range of the model. The color figure can be viewed online.

where y is the flare equivalent duration on a logarithmic scale, x is the flare total duration, and y_0 is the flare equivalent duration in the logarithmic scale for the least total duration, according to the definition of Dal & Evren (2010). It should be noted that the y_0 does not depend only on the flare mechanism, but also depends on the sensitivity of the optical system used in the mission. The most important parameter in the model is the *Plateau* value, which defines the upper limit for the flare equivalent duration on a logarithmic scale and is defined as the saturation level for a star (Dal & Evren 2011). Using the least squares method, the OPEA model leads to the results in Table 7. We plot the resulting model in Figure 8 with its 95% statistical sensitivity limit.

We tested the derived model by using method proposed by D'Agostino & Stephens (1986) to understand whether there are any other functions to model the distribution of flare equivalent durations

on this plane. In this method, the probability value (P value), is found to be ≈ 0.10, which means that there is no other function to model the distributions (Motulsky 2007; Spanier & Oldham 1987).

Ishida et al. (1991) described a frequency for the stellar flare activity as $N_1 = \Sigma n_f / \Sigma T_t$, where Σn_f is the total flare number detected in the observations, while ΣT_t is the total observing duration from the beginning of the observing season to the end. In the case of KIC 9451096 we find the N_1 frequency as 0.000368411 h^{-1} adopting the total long cadence observing duration as 1470.2786 days from the times of the first and last long cadence data points.

4. SUMMARY AND DISCUSSION

Photometric and spectroscopic analysis of KIC 9451096 reveals that the system is composed of an F5V primary and a K2V secondary star in a circular orbit with a detached binary configuration. Medium resolution TFOSC spectra suggest that the system has one third of the [Fe/H] of the Sun. Light curve modelling reasonably represents the observations. However, we are able to catch the signals of additional light variation, which is very weak compared to the variations due to the binarity and eclipses, but still observable due to the very high precision of the *Kepler* photometry.

We observe occasional flares and rotational modulation of the light curve residuals from the eclipsing binary model. Considering the physical and atmospheric properties of the components, we attribute these variations to the secondary component, which is a perfect candidate for magnetic star spot activity with its deep convective zone owing to its spectral type and very fast rotation caused by short orbital period. We inspect rotational modulations of the residuals to trace the photometric period of the secondary component, and analyze its flare characteristics.

Photometric period analysis via $O-C$ diagrams shows that the average photometric period is shorter than the orbital period by $\approx 0.5\%$ day. Under any type of differential rotation assumption (either solar like, or anti–solar like), this means that the orbital period does not correspond to the equatorial rotation period of the star. Following the method proposed by Hall & Busby (1990), we find an average differential rotation coefficient of $k = 0.069 \pm 0.008$, suggesting ≈ 3 times weaker differential rotation compared to the solar value of 0.19. We note that the type of differential rotation cannot be determined from photometry alone and we implicitly assume a solar type differential rotation in the case of KIC 9451096. However, the $k = 0.069$ value, which is extracted from very high precision continuous photometry for a restricted time range (four years in our case), defines a lower limit for the strength of the differential rotation of the star. A quick comparison of k values for other stars can be done by looking at the 17 stars listed in Hall & Busby (1990), where k values are usually a few percent or less, except for BY Dra with $k = 0.17$.

A more reliable way of detecting differential rotation with its magnitude and type is Doppler imaging, which is based on high resolution time series spectroscopy. Considering other stars whose k values were determined by Doppler imaging, we see mostly weak differential rotation with a k value of a few percent, both among solar type differential rotators (HD 208472 $k = 0.015$ (Özdarcan et al. 2016), XX Tri $k = 0.016$ (Künstler et al. 2015), ζ And $k = 0.055$ (Kővári et al. 2012), KU Peg $k = 0.04$ (Kővári et al. 2016)) and among anti–solar type differential rotators (UZ Lib $k = -0.004$ (Vida et al. 2007), σ Gem $k = -0.04$ (Kővári et al. 2015), HU Vir $k = -0.029$ (Harutyunyan et al. 2016)). Due to the binary nature of KIC 9451096, a considerable effect of tidal forces on the redistribution of the angular momentum in the convective envelope of the components can be expected, which would alter the magnitude of differential rotation (Scharlemann 1982). Based on observational findings, Collier Cameron (2007) suggests suppression of differential rotation by tidal locking, which is possibly in progress for KIC 9451096.

We detect 13 flares in the residuals from long cadence data, which are attributed to the secondary component with a corresponding $B-V$ value of $0^m.92$ (Gray 2005). We apply the OPEA model to analyze flare characteristic and find that the calculated flare parameters and resulting OPEA model parameters seem to be in agreement with parameters derived from stars analogous to the secondary component, except for the half–time value. A possible source of disagreement for the half–time value is that there are not enough sample flares at the beginning of the OPEA model.

We find an N_1 value of 0.000368411 h^{-1} for KIC 9451096. N_1 was found to be 0.41632 h^{-1} for KIC 09641031 (Yoldaş & Dal 2016), 0.01351 h^{-1} for KIC 09761199 (Yoldaş & Dal 2017), and 0.02726 h^{-1} for Group 1 and 0.01977 h^{-1} for Group 2 of KIC 2557430 (Kamil & Dal 2017). Among these sys-

tems, KIC 9451096 has the lowest N_1 value, which indicates that the magnetic activity level of the secondary component of KIC 9451096 is the lowest, according to Dal & Evren (2011).

We thank TÜBİTAK for partial support in using RTT150 (Russian-Turkish 1.5-m telescope in Antalya) with project number 14BRTT150-667. This paper includes data collected by the Kepler mission. Funding for the Kepler mission is provided by the NASA Science Mission Directorate.

APPENDIX

A.1. $O-C$ ANALYSIS RESULTS

We tabulate $O-C$ analysis results in Table 8. N is the number of the minimum, beginning from the first observed minimum in the data set. E is the decimal cycle number and E *rounded* is the rounded E number to the nearest integer or half integer. Note that as time progress $O-C$ differences approach a cycle. When this the occurs, one needs to add an additional increment of 0.5 to the E *rounded* value in order to see $O-CI$ diagram on a trend without any discontinuity.

TABLE 8

$O-C$ ANALYSIS RESULTS

N	BJD (24 00000+)	E	E $rounded$	$O-CI$ (day)	$O-CII$ (day)	N	BJD (24 00000+)	E	E $rounded$	$O-CI$ (day)	$O-CII$ (day)
1	54954.3397	-0.01	0.0	0.037559	0.378738	73	55058.7485	83.49	84.0	-0.587093	0.170127
2	54955.5840	0.98	1.0	0.031503	0.377636	74	55059.9785	84.47	85.0	-0.607518	0.154654
3	54956.8162	1.97	2.0	0.013253	0.364338	75	55061.1873	85.44	86.0	-0.649122	0.118004
4	54958.0797	2.98	3.0	0.026397	0.382435	76	55066.1529	89.41	90.0	-0.685052	0.101885
5	54959.3084	3.96	4.0	0.004684	0.365675	77	55067.4011	90.41	91.0	-0.687308	0.104582
6	54960.5831	4.98	5.0	0.028962	0.394906	78	55068.6338	91.39	92.0	-0.705006	0.091837
7	54961.8311	5.98	6.0	0.026601	0.397497	79	55069.8833	92.39	93.0	-0.705847	0.095948
8	54965.5429	8.95	9.0	-0.012834	0.372921	80	55071.1320	93.39	94.0	-0.707572	0.099177
9	54966.7917	9.94	10.0	-0.014400	0.376308	81	55072.3928	94.40	95.0	-0.697178	0.114523
10	54968.0426	10.94	11.0	-0.013919	0.381742	82	55073.6453	95.40	96.0	-0.695042	0.121612
11	54969.2711	11.93	12.0	-0.035832	0.364781	83	55074.9064	96.41	97.0	-0.684360	0.137247
12	54970.5301	12.93	13.0	-0.027244	0.378323	84	55076.1196	97.38	98.0	-0.721625	0.104935
13	54971.7622	13.92	14.0	-0.045532	0.364987	85	55077.3677	98.38	99.0	-0.723868	0.107644
14	54973.0157	14.92	15.0	-0.042376	0.373097	86	55078.6214	99.38	100.0	-0.720625	0.115841
15	54974.2711	15.93	16.0	-0.037394	0.383031	87	55079.8524	100.36	101.0	-0.739938	0.101480
16	54975.5424	16.94	17.0	-0.016495	0.408883	88	55081.1133	101.37	102.0	-0.729506	0.116866
17	54976.7582	17.92	18.0	-0.051121	0.379210	89	55082.3594	102.37	103.0	-0.733732	0.117592
18	54978.0108	18.92	19.0	-0.048923	0.386361	90	55083.6067	103.37	104.0	-0.736889	0.119388
19	54979.2462	19.90	20.0	-0.063908	0.376328	91	55084.8310	104.35	105.0	-0.762963	0.098267
20	54980.5036	20.91	21.0	-0.056872	0.388318	92	55086.1013	105.36	106.0	-0.743025	0.123158
21	54981.7375	21.90	22.0	-0.073396	0.376746	93	55094.7741	112.30	113.0	-0.823060	0.077792
22	54982.9940	22.90	23.0	-0.067271	0.387824	94	55096.0183	113.29	114.0	-0.829243	0.076563
23	54984.2387	23.90	24.0	-0.073003	0.387045	95	55097.2744	114.30	115.0	-0.823548	0.087210
24	54985.4801	24.89	25.0	-0.081962	0.383039	96	55098.4829	115.26	116.0	-0.865443	0.050269
25	54986.7385	25.90	26.0	-0.074023	0.395930	97	55102.2238	118.26	119.0	-0.875730	0.054840
26	54987.9747	26.89	27.0	-0.088237	0.386670	98	55103.4779	119.26	120.0	-0.872063	0.063460
27	54989.2224	27.88	28.0	-0.090861	0.388998	99	55104.7113	120.25	121.0	-0.889036	0.051439
28	54990.4801	28.89	29.0	-0.083562	0.401251	100	55105.9617	121.25	122.0	-0.889065	0.056364
29	54991.7160	29.88	30.0	-0.098088	0.391677	101	55107.1998	122.24	123.0	-0.901346	0.049035
30	54992.9545	30.87	31.0	-0.109983	0.384735	102	55108.4680	123.25	124.0	-0.883525	0.071809
31	54994.1980	31.86	32.0	-0.116895	0.382776	103	55109.7219	124.25	125.0	-0.880072	0.080215
32	54995.4493	32.86	33.0	-0.115976	0.388648	104	55110.9729	125.25	126.0	-0.879402	0.085838
33	54996.6932	33.86	34.0	-0.122437	0.387139	105	55112.2163	126.25	127.0	-0.886467	0.083725
34	55004.1716	39.84	40.0	-0.146475	0.392819	106	55115.9232	129.21	130.0	-0.930695	0.054357
35	55005.3983	40.82	41.0	-0.170123	0.374124	107	55117.1913	130.23	131.0	-0.913059	0.076945
36	55006.6502	41.82	42.0	-0.168696	0.380504	108	55118.4321	131.22	132.0	-0.922596	0.072361
37	55007.8905	42.81	43.0	-0.178787	0.375366	109	55119.6639	132.20	133.0	-0.941263	0.058647
38	55009.1251	43.80	44.0	-0.194516	0.364590	110	55120.9037	133.20	134.0	-0.951789	0.053074
39	55010.3779	44.80	45.0	-0.192162	0.371896	111	55122.1667	134.21	135.0	-0.939179	0.070636
40	55011.6258	45.80	46.0	-0.194622	0.374390	112	55125.8541	137.15	138.0	-1.003025	0.021649
41	55012.8550	46.78	47.0	-0.215858	0.358106	113	55127.0843	138.14	139.0	-1.023189	0.006438
42	55019.1204	51.79	52.0	-0.202426	0.396303	114	55128.3384	139.14	140.0	-1.019523	0.015057
43	55020.3475	52.78	53.0	-0.225773	0.377908	115	55129.5583	140.12	141.0	-1.050067	-0.010535
44	55021.6086	53.78	54.0	-0.215099	0.393535	116	55130.7947	141.11	142.0	-1.064060	-0.019574
45	55022.8554	54.78	55.0	-0.218692	0.394895	117	55132.0135	142.08	143.0	-1.095642	-0.046204
46	55024.1181	55.79	56.0	-0.206306	0.412234	118	55133.2565	143.07	144.0	-1.102987	-0.048595
47	55025.3559	56.78	57.0	-0.218929	0.404564	119	55134.4648	144.04	145.0	-1.145085	-0.085741
48	55026.5982	57.77	58.0	-0.227020	0.401426	120	55135.7251	145.05	146.0	-1.135194	-0.070897
49	55027.8428	58.77	59.0	-0.232822	0.400576	121	55136.9848	146.06	147.0	-1.125890	-0.056640
50	55029.0872	59.77	60.0	-0.238863	0.399489	122	55138.2260	147.05	148.0	-1.135135	-0.060932
51	55030.3152	60.75	61.0	-0.261241	0.382063	123	55139.3961	147.98	149.0	-1.215360	-0.136205
52	55031.5630	61.75	62.0	-0.263886	0.384371	124	55140.6664	149.00	150.0	-1.195475	-0.111366
53	55032.8374	62.76	63.0	-0.239869	0.413341	125	55141.9514	150.03	151.0	-1.160879	-0.071817
54	55034.0580	63.74	64.0	-0.269684	0.388479	126	55143.6087	151.35	152.5	-1.379206	-0.282715
55	55035.2816	64.72	65.0	-0.296409	0.366706	127	55144.7802	152.29	153.5	-1.458106	-0.356662
56	55036.5589	65.74	66.0	-0.269523	0.398546	129	55148.5363	155.29	156.5	-1.453207	-0.336905
57	55037.7875	66.72	67.0	-0.291324	0.381697	130	55151.0239	157.28	158.5	-1.466431	-0.340223
58	55039.0026	67.70	68.0	-0.326650	0.351324	131	55152.2748	158.28	159.5	-1.465906	-0.334745
59	55040.2237	68.67	69.0	-0.355947	0.326980	128	55146.0738	153.33	154.5	-1.414879	-0.308483
60	55041.4737	69.67	70.0	-0.356277	0.331603	132	55158.0603	162.91	164.0	-1.307165	-0.153716
61	55042.7426	70.69	71.0	-0.337835	0.354998	133	55159.3610	163.95	165.0	-1.256856	-0.098454
62	55043.9667	71.67	72.0	-0.364077	0.333709	134	55160.6064	164.95	166.0	-1.261887	-0.098533
63	55045.1588	72.62	73.0	-0.422461	0.280277	135	55161.8491	165.94	167.0	-1.269607	-0.101299
64	55046.3730	73.59	74.0	-0.458642	0.249050	136	55163.0822	166.93	168.0	-1.286891	-0.113631
65	55047.6337	74.60	75.0	-0.448283	0.264361	137	55164.3032	167.90	169.0	-1.316294	-0.138081
66	55048.8564	75.58	76.0	-0.475977	0.241620	138	55165.6046	168.95	170.0	-1.265253	-0.082087
67	55050.0805	76.55	77.0	-0.502283	0.220267	139	55166.8299	169.92	171.0	-1.290347	-0.102228
68	55051.3086	77.54	78.0	-0.524603	0.202900	140	55168.0530	170.90	172.0	-1.317624	-0.124552
69	55052.5696	78.55	79.0	-0.513982	0.218473	141	55169.3099	171.91	173.0	-1.311137	-0.113112
70	55053.7928	79.52	80.0	-0.541189	0.196220	142	55170.5385	172.89	174.0	-1.332958	-0.129981
71	55055.0220	80.51	81.0	-0.562386	0.179975	143	55171.8078	173.91	175.0	-1.314118	-0.106187
72	55057.5244	82.51	83.0	-0.560812	0.191455	144	55173.0292	174.88	176.0	-1.343042	-0.130159

TABLE 8

CONTINUED.

N	BJD (24 00000+)	E	E $rounded$	$O-CI$ (day)	$O-CII$ (day)	N	BJD (24 00000+)	E	E $rounded$	$O-CI$ (day)	$O-CII$ (day)
145	55174.2930	175.89	177.0	-1.329707	-0.111871	220	55303.6152	279.32	280.5	-1.423718	0.306739
146	55175.5226	176.88	178.0	-1.350498	-0.127709	221	55304.8802	280.33	281.5	-1.409120	0.326290
147	55176.7983	177.90	179.0	-1.325210	-0.097468	222	55306.1357	281.33	282.5	-1.404018	0.336345
148	55178.0453	178.89	180.0	-1.328543	-0.095849	223	55311.1195	285.32	286.5	-1.421824	0.338350
149	55179.2763	179.88	181.0	-1.347928	-0.110280	224	55312.3630	286.32	287.5	-1.428739	0.336388
150	55180.5189	180.87	182.0	-1.355797	-0.113197	225	55313.6050	287.31	288.5	-1.437108	0.332972
151	55181.7781	181.88	183.0	-1.347004	-0.099451	226	55314.8625	288.31	289.5	-1.430004	0.345028
152	55186.8368	185.93	187.0	-1.289813	-0.022448	227	55316.1085	289.31	290.5	-1.434445	0.345541
153	55188.0605	186.90	188.0	-1.316519	-0.044202	228	55317.3359	290.29	291.5	-1.457361	0.327577
154	55189.3531	187.94	189.0	-1.274327	0.002944	229	55318.5720	291.28	292.5	-1.471718	0.318174
155	55190.5644	188.91	190.0	-1.313459	-0.031236	230	55319.8259	292.28	293.5	-1.468206	0.326638
156	55191.8713	189.95	191.0	-1.256925	0.030251	231	55321.0985	293.30	294.5	-1.446001	0.353796
157	55193.1232	190.95	192.0	-1.255449	0.036680	232	55322.3381	294.29	295.5	-1.456806	0.347944
158	55194.3703	191.95	193.0	-1.258702	0.038380	233	55323.5690	295.28	296.5	-1.476337	0.333366
159	55195.6462	192.97	194.0	-1.233287	0.068747	234	55324.8372	296.29	297.5	-1.458487	0.356168
160	55196.8895	193.97	195.0	-1.240352	0.066636	235	55326.0951	297.30	298.5	-1.450972	0.368637
161	55198.1570	194.98	196.0	-1.223231	0.088709	236	55327.3697	298.32	299.5	-1.426734	0.397827
162	55199.3732	195.95	197.0	-1.257472	0.059421	237	55328.5737	299.28	300.5	-1.473157	0.356357
163	55200.6004	196.93	198.0	-1.280600	0.041246	238	55329.8304	300.28	301.5	-1.466867	0.367600
164	55201.8425	197.93	199.0	-1.288905	0.037894	239	55331.0867	301.29	302.5	-1.461021	0.378399
165	55203.1330	198.96	200.0	-1.248850	0.082902	240	55332.3444	302.30	303.5	-1.453717	0.390655
166	55204.3399	199.92	201.0	-1.292364	0.044341	241	55333.5987	303.30	304.5	-1.449781	0.399545
167	55205.6190	200.95	202.0	-1.263664	0.077993	242	55334.8307	304.28	305.5	-1.468202	0.386076
168	55206.9080	201.98	203.0	-1.225077	0.121534	243	55339.8133	308.27	309.5	-1.487169	0.386921
169	55208.1343	202.96	204.0	-1.249139	0.102424	244	55341.0591	309.26	310.5	-1.491789	0.387254
170	55209.4009	203.97	205.0	-1.232905	0.123611	245	55342.3111	310.27	311.5	-1.490137	0.393858
171	55210.5947	204.93	206.0	-1.289504	0.071965	246	55343.5542	311.26	312.5	-1.497472	0.391477
172	55211.8854	205.96	207.0	-1.249199	0.117223	247	55344.8142	312.27	313.5	-1.487899	0.406002
173	55213.1047	206.93	208.0	-1.280335	0.091039	248	55346.0667	313.27	314.5	-1.485736	0.413118
174	55214.3445	207.92	209.0	-1.290877	0.085451	249	55347.2510	314.22	315.5	-1.551840	0.351967
175	55215.6101	208.94	210.0	-1.275717	0.105563	250	55348.5366	315.24	316.5	-1.516661	0.392099
176	55218.0767	210.91	212.0	-1.309935	0.081251	251	55349.7558	316.22	317.5	-1.547816	0.365896
177	55219.3667	211.94	213.0	-1.270360	0.125779	252	55350.9974	317.21	318.5	-1.556621	0.362045
178	55220.5969	212.93	214.0	-1.290539	0.110553	253	55352.2301	318.20	319.5	-1.574350	0.349269
179	55221.8579	213.93	215.0	-1.279912	0.126133	254	55353.4830	319.20	320.5	-1.571818	0.356754
180	55223.0919	214.92	216.0	-1.296347	0.114650	255	55354.7468	320.21	321.5	-1.558409	0.375116
181	55224.3623	215.94	217.0	-1.276308	0.139643	256	55355.9596	321.18	322.5	-1.596054	0.342423
182	55225.5747	216.91	218.0	-1.314334	0.106569	257	55357.2235	322.19	323.5	-1.582517	0.360914
183	55226.8079	217.89	219.0	-1.331490	0.094366	258	55358.4191	323.15	324.5	-1.637362	0.311021
184	55228.0240	218.86	220.0	-1.365837	0.064972	259	55359.6607	324.14	325.5	-1.646189	0.307147
185	55229.3073	219.89	221.0	-1.332889	0.102873	260	55360.8702	325.11	326.5	-1.687083	0.271206
186	55235.6153	224.94	226.0	-1.276871	0.183655	261	55362.0811	326.08	327.5	-1.726500	0.236742
187	55236.8440	225.92	227.0	-1.298608	0.166871	262	55363.3168	327.07	328.5	-1.741265	0.226929
188	55238.1221	226.94	228.0	-1.270866	0.199566	263	55364.6085	328.10	329.5	-1.699939	0.273209
189	55239.3811	227.95	229.0	-1.262303	0.213082	264	55365.8045	329.05	330.5	-1.754329	0.223771
190	55240.6416	228.96	230.0	-1.252201	0.228136	265	55367.0570	330.06	331.5	-1.752233	0.230820
191	55241.8619	229.93	231.0	-1.282306	0.202985	266	55368.2594	331.02	332.5	-1.800184	0.187822
192	55243.1573	230.97	232.0	-1.237285	0.252958	267	55369.4948	332.01	333.5	-1.815263	0.177696
193	55244.4252	231.98	233.0	-1.219762	0.275434	268	55370.7283	332.99	334.5	-1.832084	0.165828
194	55245.6995	233.00	234.0	-1.195842	0.304307	269	55373.2283	334.99	336.5	-1.832952	0.174865
195	55246.9133	233.97	235.0	-1.232484	0.272618	270	55374.4420	335.96	337.5	-1.869624	0.143147
196	55248.1678	234.97	236.0	-1.228360	0.281694	271	55375.6859	336.96	338.5	-1.876138	0.141585
197	55249.4310	235.99	237.0	-1.215541	0.299467	272	55376.9167	337.94	339.5	-1.895727	0.126949
198	55250.6622	236.97	238.0	-1.234751	0.285209	273	55378.1620	338.94	340.5	-1.900799	0.126830
199	55251.9934	238.03	239.0	-1.154005	0.370908	274	55379.4030	339.93	341.5	-1.910187	0.122395
200	55253.2108	239.01	240.0	-1.186939	0.342927	275	55380.6643	340.94	342.5	-1.899312	0.138222
201	55255.7523	241.04	242.0	-1.146220	0.393552	276	55381.8880	341.92	343.5	-1.926050	0.116438
202	55257.0824	242.10	243.0	-1.066539	0.478186	277	55383.1384	342.92	344.5	-1.926046	0.121394
203	55259.5380	244.07	245.0	-1.111795	0.442836	278	55385.6300	344.91	346.5	-1.935183	0.122163
204	55260.7562	245.04	246.0	-1.144000	0.415583	279	55388.0983	346.88	348.5	-1.967747	0.099505
205	55261.9574	246.00	247.0	-1.193196	0.371340	280	55389.8788	348.31	350.0	-2.062848	0.011833
206	55264.5508	248.08	249.0	-1.100576	0.473866	281	55391.1218	349.30	351.0	-2.070221	0.009412
207	55286.0961	265.31	266.5	-1.437213	0.223904	282	55392.3195	350.26	352.0	-2.122895	-0.038308
208	55287.3501	266.31	267.5	-1.433601	0.232469	283	55393.5657	351.26	353.0	-2.127098	-0.037559
209	55288.6259	267.33	268.5	-1.408242	0.262781	284	55394.8151	352.26	354.0	-2.128094	-0.033602
210	55291.1470	269.35	270.5	-1.387907	0.293022	285	55396.0757	353.26	355.0	-2.117928	-0.018483
211	55292.3522	270.31	271.5	-1.433163	0.252718	286	55397.3242	354.26	356.0	-2.119832	-0.015434
212	55293.6305	271.33	272.5	-1.405215	0.285619	287	55402.3255	358.26	360.0	-2.120084	0.004126
213	55294.9054	272.35	273.5	-1.380742	0.315045	288	55403.5643	359.25	361.0	-2.131677	-0.002515
214	55296.1711	273.37	274.5	-1.365386	0.335354	289	55404.8318	360.27	362.0	-2.114591	0.019524
215	55297.3705	274.32	275.5	-1.416451	0.289241	290	55406.0530	361.24	363.0	-2.143793	-0.004725
216	55298.6338	275.34	276.5	-1.403513	0.307133	291	55407.2973	362.24	364.0	-2.149851	-0.005830
217	55299.8993	276.35	277.5	-1.388441	0.327157	292	55408.5487	363.24	365.0	-2.148882	0.000091
218	55301.1416	277.34	278.5	-1.396490	0.324062	293	55409.7850	364.23	366.0	-2.162968	-0.009041
219	55302.3750	278.33	279.5	-1.413519	0.311985	294	55412.3436	366.27	368.0	-2.105195	0.058637

TABLE 8

CONTINUED.

N	BJD (24 00000+)	E	E $rounded$	$O-CI$ (day)	$O-CII$ (day)	N	BJD (24 00000+)	E	E $rounded$	$O-CI$ (day)	$O-CII$ (day)
295	55413.5338	367.23	369.0	-2.165385	0.003400	370	55517.9911	450.77	453.0	-2.741583	-0.156757
296	55414.7921	368.23	370.0	-2.157493	0.016245	371	55519.2525	451.77	454.0	-2.730582	-0.140804
297	55416.0186	369.21	371.0	-2.181402	-0.002711	372	55527.4755	458.35	460.5	-2.635148	-0.013176
298	55416.7354	369.79	371.5	-2.089808	0.091360	373	55529.1497	459.69	462.0	-2.836493	-0.207092
299	55418.4880	371.19	373.0	-2.212791	-0.024195	374	55530.4406	460.72	463.0	-2.796050	-0.161696
300	55419.2735	371.82	373.5	-2.052432	0.138641	375	55531.1452	461.29	463.5	-2.716598	-0.079767
301	55420.9879	373.19	375.0	-2.213674	-0.015172	376	55532.3833	462.28	464.5	-2.728950	-0.087166
302	55421.7559	373.80	375.5	-2.070820	0.130159	377	55534.1421	463.68	466.0	-2.845732	-0.196520
303	55423.4753	375.18	377.0	-2.227103	-0.018694	378	55535.3509	464.65	467.0	-2.887382	-0.233216
304	55424.6650	376.13	378.0	-2.287745	-0.074384	379	55536.6507	465.69	468.0	-2.837897	-0.178779
305	55425.4776	376.78	378.5	-2.100356	0.115481	380	55537.9222	466.71	469.0	-2.816795	-0.152723
306	55426.7755	377.82	379.5	-2.052869	0.167922	381	55539.0799	467.63	470.0	-2.909571	-0.240547
307	55428.0209	378.81	380.5	-2.057878	0.167865	382	55540.3386	468.64	471.0	-2.901269	-0.227292
308	55429.2270	379.78	381.5	-2.102133	0.128563	383	55541.5096	469.58	472.0	-2.980629	-0.301699
309	55430.4917	380.79	382.5	-2.087858	0.147791	384	55546.3611	473.46	476.0	-3.130669	-0.431928
310	55434.7149	384.17	386.0	-2.241039	0.011945	385	55548.8137	475.42	478.0	-3.178938	-0.470291
311	55436.5360	385.62	387.5	-2.295580	-0.035167	386	55550.5712	476.82	479.5	-3.297044	-0.580968
312	55437.8738	386.69	388.5	-2.208186	0.057180	387	55551.2900	477.40	480.0	-3.203365	-0.484813
313	55439.6829	388.14	390.0	-2.274647	-0.001852	388	55581.3443	501.43	504.0	-3.158725	-0.321303
314	55441.5236	389.61	391.5	-2.309524	-0.029299	389	55582.5680	502.41	505.0	-3.185343	-0.342969
315	55442.8595	390.68	392.5	-2.224011	0.061166	390	55583.8233	503.42	506.0	-3.180490	-0.333162
316	55444.2076	391.76	393.5	-2.126321	0.163810	391	55585.0545	504.40	507.0	-3.199656	-0.347376
317	55445.4254	392.73	394.5	-2.158970	0.136113	392	55586.3490	505.44	508.0	-3.155569	-0.298336
318	55446.5817	393.66	395.5	-2.253082	0.046954	393	55587.5569	506.40	509.0	-3.198063	-0.335877
319	55447.7974	394.63	396.5	-2.287714	0.017275	394	55588.7810	507.38	510.0	-3.224343	-0.357204
320	55449.0846	395.66	397.5	-2.250919	0.059023	395	55590.0210	508.37	511.0	-3.234795	-0.362703
321	55450.3219	396.65	398.5	-2.264033	0.050861	396	55591.2809	509.38	512.0	-3.225287	-0.348242
322	55451.5785	397.65	399.5	-2.257797	0.062051	397	55592.5025	510.36	513.0	-3.254062	-0.372065
323	55452.8320	398.66	400.5	-2.254721	0.070079	398	55598.7504	515.35	518.0	-3.258188	-0.351426
324	55454.0597	399.64	401.5	-2.277406	0.052347	399	55599.9909	516.35	519.0	-3.268059	-0.356345
325	55455.3180	400.64	402.5	-2.269555	0.065151	400	55601.2492	517.35	520.0	-3.260152	-0.343484
326	55456.5047	401.59	403.5	-2.333185	0.006474	401	55602.4839	518.34	521.0	-3.275836	-0.354216
327	55457.7962	402.63	404.5	-2.292118	0.052494	402	55603.7203	519.33	522.0	-3.289839	-0.363266
328	55459.1257	403.69	405.5	-2.213017	0.136548	403	55604.9559	520.32	523.0	-3.304693	-0.373167
329	55460.3125	404.64	406.5	-2.276578	0.077939	404	55606.1797	521.29	524.0	-3.331256	-0.394777
330	55464.2986	407.83	410.0	-2.666942	-0.295090	405	55607.4492	522.31	525.0	-3.312166	-0.370734
331	55465.5699	408.84	411.0	-2.646049	-0.269243	406	55608.6957	523.31	526.0	-3.316053	-0.369668
332	55466.8536	409.87	412.0	-2.612669	-0.230911	407	55609.9408	524.30	527.0	-3.321311	-0.369974
333	55468.0149	410.80	413.0	-2.701802	-0.315090	408	55611.1673	525.28	528.0	-3.345244	-0.388953
334	55470.5453	412.82	415.0	-2.672173	-0.275556	409	55612.4175	526.28	529.0	-3.345435	-0.384192
335	55471.7843	413.81	416.0	-2.683608	-0.282038	410	55613.6634	527.28	530.0	-3.349928	-0.383732
336	55473.0834	414.85	417.0	-2.634861	-0.228338	411	55614.9039	528.27	531.0	-3.359846	-0.388697
337	55474.2803	415.81	418.0	-2.688400	-0.276925	412	55616.1426	529.26	532.0	-3.371578	-0.395476
338	55475.5384	416.81	419.0	-2.680723	-0.264294	413	55617.3845	530.26	533.0	-3.379993	-0.398939
339	55476.7979	417.82	420.0	-2.671646	-0.250265	414	55618.6417	531.26	534.0	-3.373253	-0.387245
340	55478.0491	418.82	421.0	-2.670770	-0.244436	415	55619.8959	532.26	535.0	-3.369461	-0.378501
341	55479.2858	419.81	422.0	-2.684507	-0.253220	416	55621.1445	533.26	536.0	-3.371252	-0.375339
342	55480.5433	420.82	423.0	-2.677432	-0.241192	417	55622.3827	534.25	537.0	-3.383398	-0.382532
343	55481.7513	421.78	424.0	-2.719789	-0.278597	418	55623.6159	535.24	538.0	-3.400672	-0.394853
344	55483.0224	422.80	425.0	-2.699057	-0.252911	419	55624.8762	536.25	539.0	-3.390707	-0.379936
345	55484.3166	423.83	426.0	-2.655281	-0.204183	420	55626.1243	537.25	540.0	-3.393051	-0.377326
346	55485.5750	424.84	427.0	-2.647331	-0.191279	421	55627.3758	538.25	541.0	-3.391897	-0.371220
347	55486.8253	425.84	428.0	-2.647428	-0.186424	422	55628.5966	539.22	542.0	-3.421553	-0.395922
348	55488.0772	426.84	429.0	-2.645888	-0.179931	423	55629.8540	540.23	543.0	-3.414508	-0.383925
349	55489.3530	427.86	430.0	-2.620526	-0.149616	424	55631.0949	541.22	544.0	-3.424005	-0.388469
350	55490.6085	428.87	431.0	-2.615342	-0.139479	425	55632.3306	542.21	545.0	-3.438666	-0.398177
351	55491.8572	429.87	432.0	-2.617035	-0.136220	426	55633.5710	543.20	546.0	-3.448712	-0.403270
352	55495.5955	432.86	435.0	-2.629946	-0.134272	427	55643.5281	551.16	554.0	-3.494757	-0.409692
353	55496.8427	433.85	436.0	-2.633212	-0.132585	428	55644.7604	552.15	555.0	-3.512933	-0.422916
354	55498.1011	434.86	437.0	-2.625201	-0.119621	429	55646.0277	553.16	556.0	-3.496032	-0.401061
355	55499.3531	435.86	438.0	-2.623584	-0.113052	430	55647.2868	554.17	557.0	-3.487318	-0.387395
356	55500.5872	436.85	439.0	-2.639858	-0.124372	431	55648.5058	555.15	558.0	-3.518696	-0.413820
357	55501.8126	437.83	440.0	-2.664902	-0.144464	432	55649.7353	556.13	559.0	-3.539555	-0.429726
358	55503.0629	438.83	441.0	-2.664999	-0.139607	433	55650.9830	557.13	560.0	-3.542329	-0.427547
359	55504.3308	439.84	442.0	-2.647460	-0.117116	434	55652.2221	558.12	561.0	-3.553545	-0.433811
360	55505.5864	440.85	443.0	-2.642238	-0.106941	435	55653.4724	559.12	562.0	-3.553676	-0.428988
361	55506.8112	441.83	444.0	-2.667895	-0.127645	436	55654.7228	560.12	563.0	-3.553646	-0.424006
362	55508.0612	442.82	445.0	-2.668225	-0.123022	437	55655.9426	561.09	564.0	-3.584330	-0.449737
363	55509.2961	443.81	446.0	-2.683800	-0.133645	438	55657.1933	562.09	565.0	-3.583949	-0.444403
364	55510.5327	444.80	447.0	-2.697541	-0.142432	439	55658.4328	563.08	566.0	-3.594841	-0.450342
365	55511.7750	445.79	448.0	-2.705675	-0.145614	440	55659.6700	564.07	567.0	-3.608046	-0.458595
366	55513.0109	446.78	449.0	-2.720178	-0.155164	441	55660.9258	565.08	568.0	-3.602692	-0.448287
367	55514.2479	447.77	450.0	-2.733544	-0.163577	442	55668.3005	570.98	574.0	-3.730384	-0.546262
368	55515.5140	448.79	451.0	-2.717896	-0.142976	443	55669.5659	571.99	575.0	-3.715347	-0.526273
369	55516.7381	449.76	452.0	-2.744146	-0.164274	444	55670.7910	572.97	576.0	-3.740715	-0.546687

TABLE 8

CONTINUED.

N	BJD (24 00000+)	E	E $rounded$	$O-CI$ (day)	$O-CII$ (day)	N	BJD (24 00000+)	E	E $rounded$	$O-CI$ (day)	$O-CII$ (day)
445	55672.0392	573.97	577.0	-3.742839	-0.543859	520	55777.4750	658.29	661.5	-3.965734	-0.348237
446	55673.2782	574.96	578.0	-3.754269	-0.550336	521	55778.6556	659.23	662.5	-4.035587	-0.413136
447	55674.5497	575.97	579.0	-3.733167	-0.524281	522	55779.9374	660.26	663.5	-4.004147	-0.376744
448	55675.7751	576.95	580.0	-3.758155	-0.544316	523	55781.1760	661.25	664.5	-4.015915	-0.383559
449	55677.0132	577.94	581.0	-3.770474	-0.551683	524	55782.4392	662.26	665.5	-4.003146	-0.365837
450	55679.5056	579.94	583.0	-3.778906	-0.550209	525	55783.6684	663.24	666.5	-4.024331	-0.382069
451	55680.7358	580.92	584.0	-3.799012	-0.565361	526	55784.9096	664.23	667.5	-4.033539	-0.386325
452	55681.9865	581.92	585.0	-3.798790	-0.560187	527	55786.1128	665.20	668.5	-4.080768	-0.428600
453	55683.2336	582.92	586.0	-3.802057	-0.558501	528	55787.3709	666.20	669.5	-4.073039	-0.415919
454	55684.4673	583.91	587.0	-3.818739	-0.570230	529	55788.6597	667.23	670.5	-4.034615	-0.372542
455	55685.7240	584.91	588.0	-3.812461	-0.558999	530	55789.9108	668.23	671.5	-4.033906	-0.366880
456	55686.9435	585.89	589.0	-3.843358	-0.584944	531	55791.1424	669.22	672.5	-4.052701	-0.380722
457	55688.1982	586.89	590.0	-3.839052	-0.575684	532	55792.3788	670.21	673.5	-4.066686	-0.389755
458	55689.4453	587.89	591.0	-3.842361	-0.574041	533	55793.6636	671.24	674.5	-4.032282	-0.350397
459	55690.6758	588.87	592.0	-3.862246	-0.588973	534	55794.8977	672.22	675.5	-4.048652	-0.361815
460	55691.9359	589.88	593.0	-3.852539	-0.574313	535	55796.1617	673.23	676.5	-4.034989	-0.343198
461	55693.1787	590.87	594.0	-3.860107	-0.576928	536	55797.4057	674.23	677.5	-4.041410	-0.344667
462	55694.4224	591.87	595.0	-3.866834	-0.578703	537	55798.6541	675.23	678.5	-4.043454	-0.341758
463	55695.6716	592.87	596.0	-3.868049	-0.574964	538	55799.9019	676.22	679.5	-4.046060	-0.339411
464	55696.9052	593.85	597.0	-3.884859	-0.586822	539	55804.8801	680.21	683.5	-4.069391	-0.342931
465	55698.1597	594.86	598.0	-3.880750	-0.577759	540	55806.1352	681.21	684.5	-4.064661	-0.333248
466	55699.4078	595.85	599.0	-3.883081	-0.575138	541	55807.3820	682.21	685.5	-4.068297	-0.331931
467	55700.6527	596.85	600.0	-3.888572	-0.575676	542	55808.6003	683.18	686.5	-4.100371	-0.359052
468	55701.8914	597.84	601.0	-3.900224	-0.582375	543	55809.8736	684.20	687.5	-4.077548	-0.331277
469	55703.1369	598.84	602.0	-3.905170	-0.582368	544	55811.1142	685.19	688.5	-4.087271	-0.336046
470	55704.3829	599.83	603.0	-3.909505	-0.581750	545	55812.3607	686.19	689.5	-4.091230	-0.335053
471	55705.6270	600.83	604.0	-3.915857	-0.583149	546	55813.6079	687.19	690.5	-4.094420	-0.333289
472	55709.3602	603.81	607.0	-3.933865	-0.586298	547	55814.8534	688.18	691.5	-4.099320	-0.333237
473	55710.6024	604.81	608.0	-3.942032	-0.589513	548	55816.1152	689.19	692.5	-4.087914	-0.316878
474	55711.8473	605.80	609.0	-3.947569	-0.590097	549	55817.3590	690.19	693.5	-4.094497	-0.318508
475	55713.0979	606.80	610.0	-3.947284	-0.584859	550	55818.6007	691.18	694.5	-4.103160	-0.322218
476	55714.3413	607.80	611.0	-3.954276	-0.586898	551	55819.8583	692.18	695.5	-4.095958	-0.310064
477	55715.5902	608.80	612.0	-3.955799	-0.583468	552	55821.0988	693.18	696.5	-4.105907	-0.315059
478	55716.7955	609.76	613.0	-4.000947	-0.623663	553	55822.3616	694.19	697.5	-4.093458	-0.297658
479	55718.0803	610.79	614.0	-3.966487	-0.584251	554	55823.5986	695.18	698.5	-4.106895	-0.306142
480	55719.3199	611.78	615.0	-3.977339	-0.590149	555	55824.8439	696.17	699.5	-4.111979	-0.306273
481	55720.5757	612.78	616.0	-3.971862	-0.579720	556	55826.0889	697.17	700.5	-4.117338	-0.306679
482	55721.8222	613.78	617.0	-3.975781	-0.578686	557	55827.3223	698.15	701.5	-4.134394	-0.318783
483	55723.0607	614.77	618.0	-3.987741	-0.585693	558	55828.5571	699.14	702.5	-4.150029	-0.329464
484	55724.3041	615.77	619.0	-3.994666	-0.587665	559	55829.8183	700.15	703.5	-4.139226	-0.313709
485	55725.5416	616.75	620.0	-4.007639	-0.595686	560	55831.0865	701.16	704.5	-4.121346	-0.290875
486	55726.8124	617.77	621.0	-3.987213	-0.570306	561	55832.3616	702.18	705.5	-4.096683	-0.261260
487	55728.0573	618.77	622.0	-3.992656	-0.570797	562	55836.0695	705.15	708.5	-4.139945	-0.289663
488	55729.3144	619.77	623.0	-3.985975	-0.559163	563	55837.2483	706.09	709.5	-4.211547	-0.356313
489	55730.5438	620.76	624.0	-4.007045	-0.575280	564	55838.4758	707.07	710.5	-4.234462	-0.374274
490	55732.4818	622.31	625.5	-3.944547	-0.505353	565	55839.7013	708.05	711.5	-4.259344	-0.394204
491	55733.7227	623.30	626.5	-3.954064	-0.509917	566	55840.9548	709.06	712.5	-4.256283	-0.386190
492	55734.9837	624.31	627.5	-3.943470	-0.494370	567	55842.0783	709.95	713.5	-4.383207	-0.508161
493	55736.2472	625.32	628.5	-3.930382	-0.476330	568	55844.5589	711.94	715.5	-4.403345	-0.518394
494	55737.4850	626.31	629.5	-3.943015	-0.484009	569	55845.7981	712.93	716.5	-4.414531	-0.524626
495	55741.2411	629.31	632.5	-3.938125	-0.464261	570	55847.0291	713.91	717.5	-4.433979	-0.539122
496	55742.4891	630.31	633.5	-3.940493	-0.461676	571	55848.2614	714.90	718.5	-4.452056	-0.552245
497	55743.7566	631.32	634.5	-3.923393	-0.439623	572	55849.5203	715.91	719.5	-4.443514	-0.538751
498	55744.9900	632.31	635.5	-3.940384	-0.451661	573	55850.7485	716.89	720.5	-4.465799	-0.556083
499	55746.2360	633.31	636.5	-3.944737	-0.451062	574	55852.0009	717.89	721.5	-4.463745	-0.549076
500	55747.4784	634.30	637.5	-3.952789	-0.454160	575	55853.2579	718.90	722.5	-4.457169	-0.537547
501	55748.7477	635.31	638.5	-3.933855	-0.430274	576	55854.5035	719.89	723.5	-4.461977	-0.537403
502	55750.0020	636.32	639.5	-3.929971	-0.421437	577	55855.7337	720.88	724.5	-4.482161	-0.552633
503	55751.2256	637.30	640.5	-3.956746	-0.443259	578	55856.9905	721.88	725.5	-4.475715	-0.541235
504	55752.4763	638.30	641.5	-3.956432	-0.437992	579	55858.2393	722.88	726.5	-4.477348	-0.537915
505	55753.7244	639.29	642.5	-3.958768	-0.435376	580	55859.4959	723.88	727.5	-4.471125	-0.526739
506	55754.9435	640.27	643.5	-3.990083	-0.461737	581	55860.7482	724.89	728.5	-4.469246	-0.519907
507	55756.1762	641.25	644.5	-4.007803	-0.474505	582	55862.0013	725.89	729.5	-4.466536	-0.512245
508	55757.4164	642.25	645.5	-4.018012	-0.479761	583	55863.2588	726.89	730.5	-4.459396	-0.500151
509	55758.6443	643.23	646.5	-4.040511	-0.497307	584	55864.5042	727.89	731.5	-4.464399	-0.500202
510	55759.8702	644.21	647.5	-4.064944	-0.516787	585	55867.0033	729.89	733.5	-4.466130	-0.492027
511	55761.1489	645.23	648.5	-4.036687	-0.483577	586	55868.2507	730.89	734.5	-4.469163	-0.490107
512	55762.4033	646.23	649.5	-4.032662	-0.474599	587	55869.5336	731.91	735.5	-4.436606	-0.452597
513	55763.6417	647.23	650.5	-4.044670	-0.481655	588	55870.7854	732.91	736.5	-4.435214	-0.446252
514	55764.8640	648.20	651.5	-4.072804	-0.504835	589	55872.0303	733.91	737.5	-4.440707	-0.446793
515	55766.1173	649.21	652.5	-4.069813	-0.496892	590	55873.3042	734.93	738.5	-4.417274	-0.418406
516	55767.4166	650.24	653.5	-4.020924	-0.443050	591	55874.5629	735.93	739.5	-4.408967	-0.405147
517	55768.7335	651.30	654.5	-3.954481	-0.371654	592	55875.8088	736.93	740.5	-4.413450	-0.404677
518	55773.7133	655.28	658.5	-3.976290	-0.373651	593	55877.0489	737.92	741.5	-4.423762	-0.410036
519	55774.9532	656.27	659.5	-3.986789	-0.379198	594	55878.3128	738.93	742.5	-4.410214	-0.391535

TABLE 8

CONTINUED.

N	BJD (24 00000+)	E	E $rounded$	$O-CI$ (day)	$O-CII$ (day)	N	BJD (24 00000+)	E	E $rounded$	$O-CI$ (day)	$O-CII$ (day)
595	55879.5416	739.92	743.5	-4.431851	-0.408220	670	56003.7288	839.23	843.0	-4.659245	-0.142803
596	55880.7939	740.92	744.5	-4.429957	-0.401372	671	56004.9865	840.24	844.0	-4.651978	-0.130584
597	55882.0707	741.94	745.5	-4.403528	-0.369991	672	56006.2124	841.22	845.0	-4.676453	-0.150105
598	55883.3312	742.95	746.5	-4.393370	-0.354879	673	56007.4532	842.21	846.0	-4.686087	-0.154787
599	55884.5770	743.94	747.5	-4.398030	-0.354587	674	56008.7066	843.22	847.0	-4.683023	-0.146770
600	55885.8409	744.95	748.5	-4.384496	-0.336100	675	56009.9833	844.24	848.0	-4.656750	-0.115544
601	55887.0573	745.93	749.5	-4.418546	-0.365197	676	56011.2389	845.24	849.0	-4.651573	-0.105414
602	55888.3593	746.97	750.5	-4.366891	-0.308589	677	56012.4835	846.24	850.0	-4.657366	-0.106255
603	55889.5836	747.95	751.5	-4.392985	-0.329731	678	56013.7525	847.25	851.0	-4.638719	-0.082654
604	55890.8943	749.00	752.5	-4.332688	-0.264480	679	56017.4903	850.24	854.0	-4.652179	-0.081256
605	55892.1496	750.00	753.5	-4.327781	-0.254621	680	56018.7292	851.23	855.0	-4.663614	-0.087738
606	55893.4424	751.03	754.5	-4.285431	-0.207318	681	56019.9859	852.24	856.0	-4.657367	-0.076538
607	55894.7718	752.10	755.5	-4.206408	-0.123342	682	56021.2562	853.25	857.0	-4.637416	-0.051634
608	55898.5258	755.10	758.5	-4.203630	-0.105705	683	56022.4634	854.22	858.0	-4.680641	-0.089907
609	55899.7909	756.11	759.5	-4.188855	-0.085978	684	56023.7186	855.22	859.0	-4.675812	-0.080124
610	55901.0305	757.10	760.5	-4.199700	-0.091869	685	56024.9527	856.21	860.0	-4.692161	-0.091521
611	55902.3176	758.13	761.5	-4.162968	-0.050185	686	56026.2011	857.21	861.0	-4.694130	-0.088537
612	55908.5262	763.10	766.5	-4.206374	-0.068826	687	56027.4389	858.20	862.0	-4.706729	-0.096183
613	55909.7727	764.09	767.5	-4.210252	-0.067752	688	56028.7216	859.22	863.0	-4.674473	-0.058974
614	55911.0224	765.09	768.5	-4.211024	-0.063571	689	56029.9668	860.22	864.0	-4.679613	-0.059162
615	55912.2796	766.10	769.5	-4.204183	-0.051777	690	56031.2015	861.21	865.0	-4.695305	-0.069900
616	55913.5339	767.10	770.5	-4.200273	-0.042914	691	56032.4606	862.21	866.0	-4.686645	-0.056288
617	55914.7453	768.07	771.5	-4.239291	-0.076980	692	56033.7172	863.22	867.0	-4.680448	-0.045137
618	55916.0044	769.08	772.5	-4.230569	-0.063304	693	56034.9441	864.20	868.0	-4.703981	-0.063718
619	55917.2754	770.09	773.5	-4.210018	-0.037800	694	56036.1521	865.17	869.0	-4.746343	-0.101127
620	55918.5032	771.08	774.5	-4.232545	-0.055374	695	56037.3725	866.14	870.0	-4.776298	-0.126129
621	55919.7735	772.09	775.5	-4.212697	-0.030573	696	56038.6342	867.15	871.0	-4.765002	-0.109880
622	55921.0127	773.08	776.5	-4.223863	-0.036787	697	56039.8562	868.13	872.0	-4.793392	-0.133318
623	55922.2473	774.07	777.5	-4.239673	-0.047643	698	56041.0903	869.11	873.0	-4.809744	-0.144716
624	55923.5184	775.09	778.5	-4.218959	-0.021977	699	56042.3999	870.16	874.0	-4.750507	-0.080527
625	55924.7604	776.08	779.5	-4.227407	-0.025472	700	56043.5881	871.11	875.0	-4.812716	-0.137783
626	55925.9988	777.07	780.5	-4.239359	-0.032471	701	56044.8140	872.09	876.0	-4.837255	-0.157369
627	55927.2605	778.08	781.5	-4.228033	-0.016192	702	56046.1021	873.12	877.0	-4.799505	-0.114666
628	55928.5484	779.11	782.5	-4.190597	0.026196	703	56047.3245	874.10	878.0	-4.827535	-0.137744
629	55931.0108	781.08	784.5	-4.228919	-0.002220	704	56049.8318	876.11	880.0	-4.821006	-0.121309
630	55933.5244	783.09	786.5	-4.216108	0.020497	705	56051.0940	877.12	881.0	-4.809175	-0.104524
631	55934.7527	784.07	787.5	-4.238299	0.003259	706	56052.3330	878.11	882.0	-4.820659	-0.111056
632	55936.0160	785.08	788.5	-4.225401	0.021110	707	56053.6291	879.14	883.0	-4.774880	-0.060324
633	55937.3165	786.12	789.5	-4.175293	0.076171	708	56054.8964	880.16	884.0	-4.758017	-0.038508
634	55938.4904	787.06	790.5	-4.251791	0.004625	709	56056.1299	881.14	885.0	-4.774941	-0.050479
635	55939.7313	788.05	791.5	-4.261290	0.000080	710	56057.3530	882.12	886.0	-4.802248	-0.072834
636	55940.9871	789.06	792.5	-4.255825	0.010497	711	56058.6402	883.15	887.0	-4.765363	-0.030995
637	55942.1709	790.00	793.5	-4.322439	-0.051164	712	56059.8824	884.14	888.0	-4.773584	-0.034264
638	55943.4297	791.01	794.5	-4.314047	-0.037819	713	56061.1510	885.16	889.0	-4.755420	-0.011147
639	55944.6554	791.99	795.5	-4.338752	-0.057571	714	56062.3606	886.13	890.0	-4.796169	-0.046943
640	55945.9115	793.00	796.5	-4.333034	-0.046901	715	56063.6314	887.14	891.0	-4.775804	-0.021625
641	55947.1251	793.97	797.5	-4.369877	-0.078790	716	56064.8673	888.13	892.0	-4.790336	-0.031205
642	55953.3348	798.93	802.5	-4.412087	-0.096236	717	56066.1357	889.14	893.0	-4.772272	-0.008187
643	55957.1577	801.99	805.5	-4.340471	-0.009761	718	56067.3561	890.12	894.0	-4.802329	-0.033292
644	55958.3450	802.94	806.5	-4.403555	-0.067893	719	56068.6012	891.12	895.0	-4.807584	-0.033593
645	55960.8259	804.92	808.5	-4.423452	-0.077884	720	56069.8800	892.14	896.0	-4.779169	-0.000226
646	55962.0744	805.92	809.5	-4.425328	-0.074807	721	56071.1306	893.14	897.0	-4.779011	0.004885
647	55963.7827	807.29	811.0	-4.592590	-0.234640	722	56072.3917	894.15	898.0	-4.768274	0.020575
648	55965.0661	808.31	812.0	-4.559609	-0.196706	723	56073.6428	895.15	899.0	-4.767540	0.026262
649	55966.2756	809.28	813.0	-4.600497	-0.232642	724	56074.8781	896.14	900.0	-4.782667	0.016087
650	55967.0586	809.91	813.5	-4.442718	-0.072386	725	56076.1587	897.16	901.0	-4.752438	0.051270
651	55968.8148	811.31	815.0	-4.562135	-0.184374	726	56077.4056	898.16	902.0	-4.756028	0.052632
652	55970.0661	812.31	816.0	-4.561169	-0.178455	727	56079.8767	900.13	904.0	-4.785636	0.032930
653	55971.2856	813.29	817.0	-4.592106	-0.204439	728	56081.1116	901.12	905.0	-4.801164	0.022355
654	55972.5454	814.30	818.0	-4.582676	-0.190056	729	56082.3635	902.12	906.0	-4.799698	0.028773
655	55973.7539	815.26	819.0	-4.624577	-0.227005	730	56083.6313	903.14	907.0	-4.782319	0.051106
656	55975.0214	816.28	820.0	-4.607483	-0.204957	731	56084.9003	904.15	908.0	-4.763703	0.074674
657	55976.2771	817.28	821.0	-4.602175	-0.194697	732	56086.1298	905.14	909.0	-4.784578	0.058753
658	55977.5314	818.28	822.0	-4.598299	-0.185868	733	56087.5015	906.23	910.0	-4.663248	0.185035
659	55978.7643	819.27	823.0	-4.615758	-0.198374	734	56088.6842	907.18	911.0	-4.730959	0.122277
660	55979.9747	820.24	824.0	-4.655789	-0.233452	735	56089.9448	908.19	912.0	-4.720742	0.137447
661	55981.2152	821.23	825.0	-4.665663	-0.238373	736	56091.2300	909.21	913.0	-4.685964	0.177178
662	55982.4649	822.23	826.0	-4.666399	-0.234156	737	56092.5058	910.23	914.0	-4.660525	0.207569
663	55983.7136	823.23	827.0	-4.668098	-0.230903	738	56093.7745	911.25	915.0	-4.642299	0.230749
664	55984.9510	824.22	828.0	-4.681100	-0.238951	739	56094.9799	912.21	916.0	-4.687304	0.190696
665	55989.9800	828.24	832.0	-4.653728	-0.191768	740	56096.2424	913.22	917.0	-4.675205	0.207748
666	55991.2123	829.22	833.0	-4.671806	-0.204893	741	56097.4796	914.21	918.0	-4.688382	0.199524
667	55999.9721	836.23	840.0	-4.664749	-0.163166	742	56098.7419	915.22	919.0	-4.676466	0.216393
668	56001.2541	837.26	841.0	-4.633138	-0.126602	743	56100.0357	916.26	920.0	-4.633054	0.264757
669	56002.4704	838.23	842.0	-4.667280	-0.155791	744	56103.7566	919.23	923.0	-4.663377	0.249294

TABLE 8

CONTINUED.

N	BJD (24 00000+)	E	E $rounded$	$O-CI$ (day)	$O-CII$ (day)	N	BJD (24 00000+)	E	E $rounded$	$O-CI$ (day)	$O-CII$ (day)
745	56109.9954	924.22	928.0	-4.676521	0.260913	820	56280.1868	1060.33	1064.5	-5.164583	0.448917
746	56113.3747	926.92	930.5	-4.423214	0.526603	821	56281.4444	1061.34	1065.5	-5.157329	0.461124
747	56114.6248	927.92	931.5	-4.423513	0.531257	822	56282.6976	1062.34	1066.5	-5.154557	0.468849
748	56115.7986	928.86	932.5	-4.500115	0.459608	823	56283.9438	1063.34	1067.5	-5.158731	0.469628
749	56117.0832	929.89	933.5	-4.465890	0.498785	824	56285.1959	1064.34	1068.5	-5.157032	0.476279
750	56118.3527	930.91	934.5	-4.446877	0.522752	825	56286.4349	1065.33	1069.5	-5.168392	0.469873
751	56119.5428	931.86	935.5	-4.507145	0.467436	826	56287.7086	1066.35	1070.5	-5.145137	0.498080
752	56120.8400	932.89	936.5	-4.460308	0.519226	827	56288.9621	1067.35	1071.5	-5.142071	0.506100
753	56130.7366	940.81	944.5	-4.566916	0.452241	828	56290.2105	1068.35	1072.5	-5.144032	0.509091
754	56131.9796	941.80	945.5	-4.574294	0.449816	829	56291.5000	1069.38	1073.5	-5.104957	0.553119
755	56133.2522	942.82	946.5	-4.552111	0.476952	830	56292.7161	1070.35	1074.5	-5.139240	0.523789
756	56134.5096	943.83	947.5	-4.545067	0.488948	831	56293.9407	1071.33	1075.5	-5.164982	0.503000
757	56135.7513	944.82	948.5	-4.553808	0.485161	832	56295.1578	1072.31	1076.5	-5.198336	0.474598
758	56137.0225	945.84	949.5	-4.532967	0.510954	833	56296.5060	1073.38	1077.5	-5.100564	0.577324
759	56140.7674	948.83	952.5	-4.539328	0.519452	834	56297.7531	1074.38	1078.5	-5.103797	0.579043
760	56141.9916	949.81	953.5	-4.565516	0.498216	835	56299.0033	1075.38	1079.5	-5.104009	0.583784
761	56143.2569	950.82	954.5	-4.550588	0.518098	836	56300.2023	1076.34	1080.5	-5.155419	0.537327
762	56144.4883	951.81	955.5	-4.569578	0.504060	837	56301.5096	1077.39	1081.5	-5.098526	0.599173
763	56145.7466	952.81	956.5	-4.561720	0.516871	838	56302.7539	1078.38	1082.5	-5.104652	0.597999
764	56146.9715	953.79	957.5	-4.587229	0.496315	839	56306.4198	1081.31	1085.5	-5.189954	0.527557
765	56148.2190	954.79	958.5	-4.590118	0.498379	840	56307.7524	1082.38	1086.5	-5.107673	0.614790
766	56149.4577	955.78	959.5	-4.601816	0.491634	841	56309.0245	1083.40	1087.5	-5.086023	0.641393
767	56150.6775	956.76	960.5	-4.632407	0.465996	842	56325.9302	1096.92	1101.0	-5.060647	0.733633
768	56151.9655	957.79	961.5	-4.594806	0.508549	843	56328.3853	1098.88	1103.0	-5.106394	0.697792
769	56153.2038	958.78	962.5	-4.606888	0.501421	844	56329.5597	1099.82	1104.0	-5.182402	0.626736
770	56154.4204	959.75	963.5	-4.640735	0.472526	845	56330.8501	1100.85	1105.0	-5.142333	0.671758
771	56155.6456	960.73	964.5	-4.665864	0.452350	846	56333.3113	1102.82	1107.0	-5.181996	0.642001
772	56156.8928	961.73	965.5	-4.669096	0.454071	847	56334.5619	1103.82	1108.0	-5.181752	0.647198
773	56158.1712	962.75	966.5	-4.641105	0.487015	848	56335.7465	1104.77	1109.0	-5.247612	0.586291
774	56159.4100	963.74	967.5	-4.652695	0.480377	849	56337.0201	1105.78	1110.0	-5.224408	0.614447
775	56208.2411	1002.79	1007.0	-5.212331	0.116379	850	56338.2570	1106.77	1111.0	-5.237886	0.605923
776	56209.4810	1003.79	1008.0	-5.222828	0.110836	851	56339.4611	1107.74	1112.0	-5.284151	0.564610
777	56210.7714	1004.82	1009.0	-5.182829	0.155787	852	56340.6906	1108.72	1113.0	-5.305020	0.548694
778	56213.3022	1006.84	1011.0	-5.152775	0.195747	853	56341.9756	1109.75	1114.5	-5.895645	-0.034501
779	56214.5478	1007.84	1012.0	-5.157621	0.195854	854	56343.2492	1110.77	1115.5	-5.872415	-0.006319
780	56215.7983	1008.84	1013.0	-5.157546	0.200882	855	56344.4293	1111.71	1116.5	-5.942756	-0.071706
781	56217.0470	1009.84	1014.0	-5.159207	0.204174	856	56345.7230	1112.74	1117.5	-5.899509	-0.023507
782	56218.2981	1010.84	1015.0	-5.158470	0.209863	857	56346.9865	1113.76	1118.5	-5.886309	-0.005354
783	56219.5546	1011.84	1016.0	-5.152404	0.220883	858	56348.2050	1114.73	1119.5	-5.918239	-0.032331
784	56220.8009	1012.84	1017.0	-5.156531	0.221708	859	56349.4638	1115.74	1120.5	-5.909852	-0.018991
785	56222.0363	1013.83	1018.0	-5.171527	0.211665	860	56350.6891	1116.72	1121.5	-5.934905	-0.039092
786	56223.2783	1014.82	1019.0	-5.179907	0.208238	861	56352.0308	1117.79	1122.5	-5.843619	0.057148
787	56224.5537	1015.84	1020.0	-5.154868	0.238230	862	56353.3171	1118.82	1123.5	-5.807787	0.097932
788	56225.8164	1016.85	1021.0	-5.142631	0.255419	863	56354.5736	1119.82	1124.5	-5.801645	0.109027
789	56227.0506	1017.84	1022.0	-5.158845	0.244159	864	56355.8250	1120.82	1125.5	-5.800643	0.114982
790	56228.3015	1018.84	1023.0	-5.158301	0.249655	865	56357.0925	1121.84	1126.5	-5.783577	0.137001
791	56229.5273	1019.82	1024.0	-5.182880	0.230030	866	56360.7909	1124.80	1129.5	-5.836365	0.099071
792	56230.8226	1020.85	1025.0	-5.138000	0.279862	867	56362.0787	1125.83	1130.5	-5.798958	0.141432
793	56232.0699	1021.85	1026.0	-5.141082	0.281733	868	56363.3212	1126.82	1131.5	-5.806816	0.138526
794	56233.2894	1022.83	1027.0	-5.171953	0.255815	869	56364.5903	1127.83	1132.5	-5.788165	0.162130
795	56234.5424	1023.83	1028.0	-5.169397	0.263324	870	56365.8475	1128.84	1133.5	-5.781346	0.173902
796	56235.7786	1024.82	1029.0	-5.183627	0.254046	871	56367.0963	1129.84	1134.5	-5.782885	0.177316
797	56239.5391	1027.82	1032.0	-5.174262	0.278270	872	56368.3384	1130.83	1135.5	-5.791247	0.173906
798	56240.7773	1028.81	1033.0	-5.186457	0.271028	873	56369.6252	1131.86	1136.5	-5.754795	0.215312
799	56242.0276	1029.81	1034.0	-5.186631	0.275807	874	56370.8651	1132.85	1137.5	-5.765300	0.209759
800	56243.2577	1030.80	1035.0	-5.206922	0.260468	875	56372.1318	1133.87	1138.5	-5.749028	0.230984
801	56244.5006	1031.79	1036.0	-5.214427	0.257917	876	56373.3682	1134.85	1139.5	-5.763039	0.221926
802	56253.3022	1038.83	1043.0	-5.165545	0.341468	877	56374.6499	1135.88	1140.5	-5.731719	0.258199
803	56254.5576	1039.84	1044.0	-5.160566	0.351401	878	56375.8468	1136.84	1141.5	-5.785202	0.209668
804	56255.8080	1040.84	1045.0	-5.160585	0.356334	879	56377.1089	1137.85	1142.5	-5.773500	0.226324
805	56257.0728	1041.85	1046.0	-5.146118	0.375754	880	56378.3842	1138.87	1143.5	-5.748615	0.256161
806	56258.3140	1042.84	1047.0	-5.155379	0.371446	881	56379.6388	1139.87	1144.5	-5.744433	0.265297
807	56259.5516	1043.83	1048.0	-5.168190	0.363588	882	56380.8733	1140.86	1145.5	-5.760302	0.254380
808	56260.7955	1044.82	1049.0	-5.174669	0.362061	883	56382.1355	1141.87	1146.5	-5.748486	0.271149
809	56262.0533	1045.83	1050.0	-5.167215	0.374469	884	56383.3994	1142.88	1147.5	-5.735011	0.289577
810	56263.2775	1046.81	1051.0	-5.193508	0.353128	885	56384.6451	1143.87	1148.5	-5.739710	0.289831
811	56264.5440	1047.82	1052.0	-5.177382	0.374208	886	56385.8893	1144.87	1149.5	-5.745889	0.288604
812	56265.7843	1048.81	1053.0	-5.187410	0.369132	887	56387.1412	1145.87	1150.5	-5.744449	0.294998
813	56267.0202	1049.80	1054.0	-5.201944	0.359551	888	56388.3931	1146.87	1151.5	-5.742949	0.301450
814	56270.7982	1052.82	1057.0	-5.175126	0.401228	889	56389.6473	1147.87	1152.5	-5.739137	0.310215
815	56272.0692	1053.84	1058.0	-5.154509	0.426798	890	56394.6352	1151.86	1156.5	-5.752815	0.316349
816	56275.1726	1056.32	1060.5	-5.177166	0.416523	891	56395.8689	1152.85	1157.5	-5.769539	0.304577
817	56276.4370	1057.33	1061.5	-5.163184	0.435458	892	56397.1298	1153.86	1158.5	-5.758961	0.320109
818	56277.6912	1058.34	1062.5	-5.159377	0.444217	893	56398.3793	1154.86	1159.5	-5.759917	0.324105
819	56278.9163	1059.32	1063.5	-5.184624	0.423924	894	56399.6365	1155.86	1160.5	-5.753126	0.335849

TABLE 8

CONTINUED.

N	BJD (24 00000+)	E	E $rounded$	$O-CI$ (day)	$O-CII$ (day)	N	BJD (24 00000+)	E	E $rounded$	$O-CI$ (day)	$O-CII$ (day)
895	56400.8789	1156.86	1161.5	-5.761061	0.332867	902	56409.6487	1163.87	1168.5	-5.744102	0.384496
896	56402.1367	1157.86	1162.5	-5.753714	0.345167	903	56410.8892	1164.86	1169.5	-5.753967	0.379583
897	56403.3823	1158.86	1163.5	-5.758478	0.345355	904	56412.1522	1165.87	1170.5	-5.741409	0.397095
898	56404.6358	1159.86	1164.5	-5.755425	0.353362	905	56413.4054	1166.87	1171.5	-5.738612	0.404844
899	56405.8873	1160.86	1165.5	-5.754252	0.359487	906	56420.9048	1172.87	1177.5	-5.741557	0.431616
900	56407.1374	1161.86	1166.5	-5.754610	0.364082	907	56422.1512	1173.87	1178.5	-5.745583	0.432544
901	56408.3847	1162.86	1167.5	-5.757700	0.365945	908	56423.4023	1174.87	1179.5	-5.744909	0.438170

REFERENCES

Armstrong, D. J., Gómez Maqueo Chew, Y., Faedi, F., & Pollacco, D. 2014, MNRAS, 437, 3473

Balona, L. A. 2015, MNRAS, 447, 2714

Balona, L. A., Švanda, M., & Karlický, M. 2016, MNRAS, 463, 1740

Blanco-Cuaresma, S., Soubiran, C., Heiter, U., & Jofré, P. 2014, A&A, 569, A111

Borkovits, T., Hajdu, T., Sztakovics, J., et al. 2016, MNRAS, 455, 4136

Castelli, F. & Kurucz, R. L. 2004, ArXiv Astrophysics e-prints

Collier Cameron, A. 2007, AN, 328, 1030

D'Agostino, R. B. & Stephens, M. A. 1986, Goodness-of-fit techniques, (New York, NY: Dekker)

Dal, H. A. & Evren, S. 2010, AJ, 140, 483

_____. 2011, AJ, 141, 33

Gershberg, R. E. 1972, Ap&SS, 19, 75

_____. 2005, Solar-Type Activity in Main-Sequence Stars, (Berlin Heidelberg: Springer)

Gray, D. F. 2005, The Observation and Analysis of Stellar Photospheres, (3rd ed; Cambridge, MA: CUP)

Gray, R. O. & Corbally, C. J. 1994, AJ, 107, 742

Hall, D. S. & Busby, M. R. 1990, ASIC 319, NATO Advanced Study Institute on Active Close Binaries, ed. C. Ibanoglu, (Durdrecht, The Netherlands: Kluwer Academic Publishers), 377

Harutyunyan, G., Strassmeier, K. G., Künstler, A., Carroll, T. A., & Weber, M. 2016, A&A, 592, A117

Hawley, S. L., Davenport, J. R. A., Kowalski, A. F., et al. 2014, ApJ, 797, 121

Ishida, K., Ichimura, K., Shimizu, Y., & Mahasenaputra. 1991, Ap&SS, 182, 227

Kamil, C. & Dal, H. A. 2017, PASA, 34, 29

Klinglesmith, D. A. & Sobieski, S. 1970, AJ, 75, 175

Kövári, Z., Korhonen, H., Kriskovics, L., et al. 2012, A&A, 539, A50

Kövári, Z., Kriskovics, L., Künstler, A., et al. 2015, A&A, 573, A98

Kövári, Z., Künstler, A., Strassmeier, K. G., et al. 2016, A&A, 596, A53

Künstler, A., Carroll, T. A., & Strassmeier, K. G. 2015, A&A, 578, A101

Leto, G., Pagano, I., Buemi, C. S., & Rodono, M. 1997, A&A, 327, 1114

Motulsky, H. 2007, GraphPad Software, 31, 39

Özdarcan, O., Carroll, T. A., Künstler, A., et al. 2016, A&A, 593, A123

Özdarcan, O., Evren, S., Strassmeier, K. G., Granzer, T., & Henry, G. W. 2010, AN, 331, 794

Prša, A., Batalha, N., Slawson, R. W., et al. 2011, AJ, 141, 83

Reinhold, T. & Reiners, A. 2013, A&A, 557, A11

Reinhold, T., Reiners, A., & Basri, G. 2013a, A&A, 560, A4

_____. 2013b, A&A, 560, A4

Ryabchikova, T., Piskunov, N., Kurucz, R. L., et al. 2015, PhyS, 90, 4005

Scharlemann, E. T. 1982, ApJ, 253, 298

Slawson, R. W., Prša, A., Welsh, W. F., et al. 2011, AJ, 142, 160

Spanier, J. & Oldham, K. B. 1987, An Atlas of Functions (Bristol, PA: Taylor & Francis/Hemisphere)

Tonry, J. & Davis, M. 1979, AJ, 84, 1511

van Hamme, W. 1993, AJ, 106, 2096

van Kerkwijk, M. H., Rappaport, S. A., Breton, R. P., et al. 2010, ApJ, 715, 51

Vida, K., Kovári, Z., Švanda, M., Oláh, K., Strassmeier, K. G., & Bartus, J. 2007, AN, 328, 1078

Wilson, R. E. & Devinney, E. J. 1971, ApJ, 166, 605

Wilson, R. E. & Van Hamme, W. 2014, ApJ, 780, 151

Yoldaş, E. & Dal, H. A. 2016, PASA, 33, e016

_____. 2017, RMxAA, 53, 67

H. A. Dal, O. Özdarcan, and E. Yoldaş: Ege University, Science Faculty, Department of Astronomy and Space Sciences, 35100 Bornova, İzmir, Turkey (orkun.ozdarcan@ege.edu.tr).